FRIEDRICH-ALEXANDER
UNIVERSITÄT
ERLANGEN-NÜRNBERG

Institute for
Multiscale Simulation
MSS

University of Erlangen-Nuremberg

Bachelor thesis

# Damping an oscillation with granular dampers

*Author:*
Jonas Rathke
Mail: jonas.rathke@fau.de

*Supervisors:*
Prof. Dr. Thorsten Pöschel
Dr. Kerstin Avila

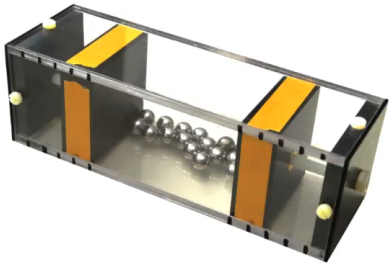

[2]

December $19^{th}$, 2014

# Eidesstattliche Erklärung

Ich versichere, dass ich die Arbeit mit dem Titel "Damping an oscillation with granular dampers" ohne fremde Hilfe und ohne Benutzung anderer als der angegebenen Quellen angefertigt habe und dass die Arbeit in gleicher oder ähnlicher Form noch keiner anderen Prüfungsbehörden vorgelegen hat und von dieser als Teil einer Prüfungsleistung angenommen wurde. Alle Ausführungen, die wörtlich oder sinngemäß übernommen wurden, sind als solche gekennzeichnet.

# Statutory Declaration

I declare that I have developed and written the enclosed thesis entitled "Damping an oscillation with granular dampers" entirely by myself and have not used sources or means without declaration in the text. Any thoughts or quotations which were inferred from these sources are clearly marked as such. This thesis was not submitted in the same or in a substantially similar version, not even partially, to any other authority to achieve an academic grading and was not published elsewhere.

Erlangen, December $19^{th}$, 2014

Unterschrift: _____
Jonas Rathke

# Preamble

Zuerst gilt mein Dank Melie, die mich während dem Studium unterstütze wo immer ich Hilfe brauchte. Ohne sie wäre ich nicht so locker und glücklich durch das Studium gekommen.

Meine Familie hat mir alles was ich jetzt habe und mache ermöglicht. Dafür bin ich ihnen unendlich dankbar und hoffe dass sie das auch wissen.

Ich möchte mich ebenfalls bei allen Menschen bedanken, die mich in den all meinen Jahren persönlich begleitet haben. Besonderer Dank geht an meine Penzberger und Erlanger Freunde, die mir stets mit Rat und Tat zur Seite standen. Viele Leute laufen mit dem Strom, ohne dabei zu wissen was um sie herum ist. Ich bin dankbar dass es mir möglich gemacht wurde, auch Blickwinkel von ausserhalb des Stromes einzunehmen.

Thanks to Dr. Kerstin Avila who committed herself to give me the best possible mentoring and to Prof. Pöschel who helped out with advice if Dr. Avila was unavailable. The boundary conditions of personal growth were made possible by them during the preparation of this thesis.

*Kites rise highest against the wind, not with it.*
-Winston Churchill

Special thanks to Michael Miller of the 'Mechanikwerkstatt der Technischen Fakultät der FAU Erlangen-Nürnberg' who helped a lot in designing and constructing the damper.

# Contents

# List of Figures

# 1 Introduction

Vibrating structures (for example buildings, bridges, skyscrapers or mobility products) are a threat to human life. Any vibrating part is more likely to brake early and cause material and environmental damage. Also costs of reparation and maintenance play a big role in vibration prevention. In the energy and chemical sector, all plants are an individual product and the process and product assurance has the highest priority in the design process.

This explains the long and costly planning phases of industry plants or consumer products. Reliability, safety and economical aspects are all taken into account and influence the design. In many complex systems where an interaction of vibrating inducers to structures occurs not all eventualities can be foreseen.

On process engineering plants, long pipe runs are installed on pipe-racks and routed to static or rotating equipment to convey fluids for various chemical process steps. Engineering companies designing the plant components are normally contractual wise bound to design the plant equipment for a specified lifetime of minimum 20-30 years and furthermore have to guarantee the operational availability of the plant per year.

Plant shutdowns have therefore to be minimized. Consequently engineering companies involved in designing the plant are taking any aspect of plant failure into account.

Applying components after construction is an interesting option but in many instances it is only possible with high investments and efforts and does not exclude more maintenance automatically.

It is the aim of this thesis to give an example of a granular damper design and application in an industrial environment where the boundary conditions are not always consistent. This damper has the purpose of damping a mechanical vibration of a fluid leading pipe.

Figure 1: Natural gas processing plant (figure taken from [3] )

# 2 Processing facility issues

## 2.1 Industrial facility outages

On process engineering plants, long pipe runs are laid on steel stands through the facilities to convey the gaseous and liquid compounds needed in multiple chemical processes. Those pipelines and the processing units are designed to last sufficiently long to return the initial investment costs of the plant.

Nevertheless, outages due to erosion, fatigue and lifetime shortening result from an advanced age-related wear. This arises for example in structural changes of material and surface of the plant components. A proper design tries to prevent such cases with regards to safety and longevity. Random failures are hard to predict since they are caused by exogenous disturbances which are not taken into account under normal operation.

Most of the random failures originate in many types of fluctuating application conditions of a facility e.g. static vibrations or abrupt load fluctuation [7, p. 59].

With regard to safety and longevity the importance of piping is reflected in the planning costs of the pipeline and can add up to 40% of the total planning costs [20, p. 6-22]. It is also reflected in the construction costs of a process plant: around 30% are budgeted for pipelines and process machines [21, p. 413-417].

To prevent the machines from braking down before the lifetime of a plant exceeds, around 2 - 4 % of the investment costs are used each year for machine and component maintenance. That includes inspection, machine care, service and repair as well as improvement of the functional reliability [53, p. 300].

In total, the cost of maintenance represent around two to three times the investment costs [53, p. 300]. This underlines the importance of a secure plant operation and planning not just to prevent human and environmental damage but also in terms of investment costs.

## 2.2 U-bend expansion joint

In thermal fluctuating ambient conditions or with pipes leading tempered fluids, thermal expansion and contraction exerts influence on the pipes. With the following formula, it is possible to calculate the expansion $\Delta L$ of a pipe with the length $L$, the coefficient of thermal expansion of the pipe material $\alpha$ and the temperature difference $\vartheta$ [48, p. 83].

$$\Delta L = \alpha \times \Delta\vartheta \times L$$

These thermal influences can result in failure of the pipe system by over-stressing the pipe material. Therefore it is necessary for plant engineers to insert e.g. expansion joints to prevent damage of the pipe system and subsequently costs of plant idleness and maintenance.

It is a standard practice to apply expansion joints (for example a u-shaped pipe, called the u-bend expansion joint) for which certain design specifications exist: it is mandatory to mount the u-bend expansion joint movably. The compulsory guide should be set up with a distance from the bend 15 to 20 times the diameter of the pipe [48, p. 97].

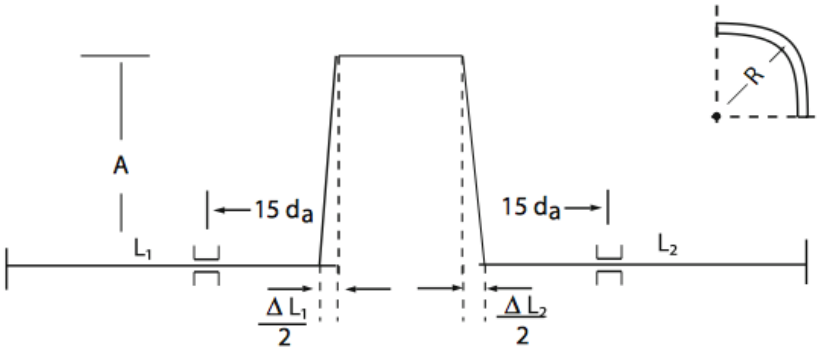


Figure 2: U-bend expansion joint movable mounting (figure taken from [48, p. 98] )

Thus the u-shaped part of the expansion loop is not mounted and hanging freely without any channeling to deliver the necessary elasticity. This makes such kind of channeling vulnerable to outside forces.

To make sure the safety of the facility is not endangered, all other loading cases have to be considered and evaluated with a strength calculation of a pipeline. Those loading cases can be pressure surges, weather influences such as wind or rain, start-up or shut-down processes or pressure fluctuations [48, p. 99].

## 2.3 Oscillating simplex pumps

To convey fluids through the pipes, so called simplex pumps are frequently utilized in heat economy and hazardous area operations. They are characterized by modesty, little required space, low asset costs as well as easy controllability. Their name simplex has its origin in the fact that they are composed of or characterized by a single part or structure [9, p. L29].

In comparison with other displacement pumps they are capable of building high pressures up to 3,500 bar but they can also act as a vibration generator.

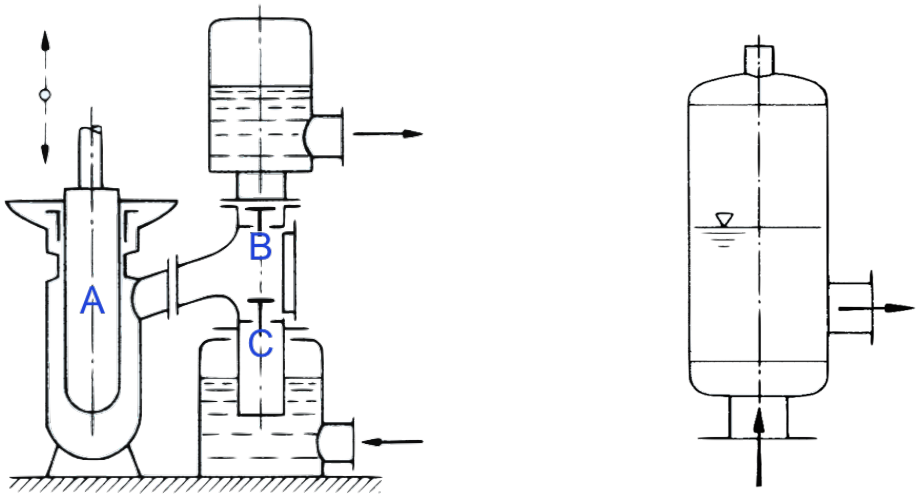


(a) (b)

Figure 3: Typical structure of a simplex pump (a) and a compressed-air chamber (b)(figure taken from [51, p. P14, P16] )

Other capabilities of oscillating simplex pumps are widespread: Their main applications are hydraulic systems, abrasives and high viscosity bulk slurry, high viscosity but non-abrasive fluids and dosing pumps [51, p. P13].

The principle of displacement underlies these pumps. The generation of the suction and compression effect is elicited by a piston (see A in Figure 3a). This plunger piston presses the water through the pressure valve (see B in Figure 3a) where it is then released into the pressure chamber subsequently. Every second stroke the water will be pressed into the pipe system. On the opposite side (see C in Figure 3a), due to atmospheric pressure, the intake stroke resqueezes water into the anteroom. [9, p. L28]

Through the back and forth movement of the plunger piston a pulsating conveyance of the working fluid is formed (see figure 13a). Most conventional pumps use a compressed-air chamber (Figure 3b) in front and after the anteroom to compensate the movement of the hydrostatic head during compression and suction processes in the pipe [9, p. L28].

The compressed-air chamber is partly filled with air. During the pressure stroke it mounts the water level. As a result, the air is compressed and the water as well as the pressure are rising inside the chamber. Pumping water into the pressure face lowers the pressure and the water-level. From time to time, a vessel can be used to refill the air buffer when it depletes [9, p. L28].

But at delivery pressures above 15 bar, the operation of the air valve is uneconomical [9, p. L28]. Hence it is necessary to integrate a pin to supply the compressed-air chamber steadily.

Other components to level the pressure and suction hydrostatic head are: bubble memories (same principle as compressed-air chamber, with a pre-compressed gas-filled balloon), resonators (damping of the compressional wave via reflexion at a change of cross section) and bezels (also damping of the compressional wave via reflexion but with high pressure losses) [51, p. P16f].

## 2.4 Combining simplex pumps and u-bends

In combination with the widespread use of oscillating simplex pumps, which ensure intermittent delivery of fluids and are reliable as well as economical for high pressures, the u-bend pipe leads to vibrations of the pipeline and eventually of the construction.

The *two-stage Woehler curve* describes the phenomena of high strength steel up to the ultra high cycle fatigue region. The strength of a material decreases over the numbers of load cycles it has to withstand [46, p. 131].

This ultra high cycle fatigue region is stressed with more than $10^7$ load cycles since the lifetime of a plant is around twenty years. If a simplex pump for example pulsates with an average of 200 revolutions per minute (which equals 200 load cycles), the u-bend pipe has to outlast around $2x10^9$ cycles. Using this *Woehler curve*, it is acted on the assumption that the decrease of the endurance strength results not because of the crack initiation on the surface but moreover of the inner structure of the part [35, p. 40-47].

For example this can be an inclusion in the pipe material or the micro structure itself, with grain size and defects playing a role in crack initiation [46, p. 132].

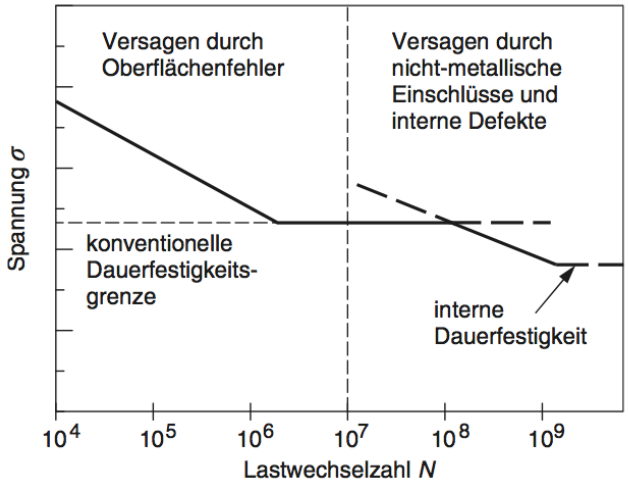


Figure 4: Two-stage Woehler curve, x-axis: load changes, y-axis: tension $\sigma$(figure taken from[46] )

In conclusion, the combination of simplex pumps and u-bends impose a threat for the reliable and continuous operation of a plant. As a consequence, it is necessary to damp vibrations in the u-bend wherever it is possible.

Occasionally, it is not possible or would increase the cost of an otherwise cheap component to damp the vibrations with the measures mentioned before. Fluid-focused damping measures can't prevent resulting mechanical resonance situations without exception even though pulsation dampers reduce the pipe oscillation to an extend [26, p. 198].

Some mechanical dampers such as rubber or spring damper can't be applied to a pipe system as for reasons mentioned in chapter 2.2 'U-bend expansion joint' and alternatives have to be found to provide a sufficient damping of the vibrations.

For the dimensioning it is necessary to consider the whole system in regard to the safety and the technical regulations of the combination of pipelines and simplex pumps. In the beginning the individual components have to meet the safety and regulation criteria and then the combination of all components in a setting has to be investigated. Otherwise, outages and disruptions might be a possible result due to a lack of engineering diligence .

The design procedure in case of a combination of pipelines and a simplex pump would be the following: At first, pressure oscillations, shaking forces and vibrations of the pipelines due to the pulsating stream that results from the pump kinematics have to be analyzed with an adequate numeric method [26, p. 198].

Secondly, design procedures would follow the operation criteria which were set up by Vetter [52] for the prevention of

- cavitation through minimum pressure warranty at the pump intake flange.
- over-suction by keeping the pressure at the pump pressure flange higher than on the intake flange.
- over-stress in order that the maximum tolerable pressure will not be exceeded at no place and at no point at any time.
- undue pulsation of the delivery rate to eliminate hydraulic or mechanical oscillations.
- mechanical resonance of the pipe system by detailed analysis.

All the criteria above have to be fulfilled to ensure a reliable and safe operation of a plant. If one is not fulfilled, corrective measures in form of additional components or a change of the pipe design have to be applied.

### 2.4.1 (Resonance)Vibration behaviour of pipe systems

The behavior of mechanical vibration depends on the boundary conditions and on the kind of excitation. The vibration in a resonance state is determined by the eigenmode of a pipeline structure. To determine them, the material characteristics and the geometry result in the eigenfrequency [26, p. 6].

Depending on the physical complexity of the pipeline, multiple vibrations overlay each other, for instance torsion and longitudinal oscillation are coupled with bending vibration.

Usually, occurring transversal bending vibration frequencies in process engineering are below 100 Hz and are responsible for most of the vibrations in processing facilities [26, p. 6]. They can be divided into three categories: longitudinal, circumference and cylinder nappe bend oscillations. The analytical description of the mechanical eigenfrequencies $w$ of a pipe can be described through the homogeneous, partial differential equation of forth order [54] [59], with $\rho$ as the density, $A$ as the area, $EI$ as mechanical parameters, $t$ as the time and $x$ as the displacement respectively:

$$\frac{\rho A}{EI}\frac{\delta^2 w}{\delta t^2} + \frac{\delta^4 w}{\delta x^4} = 0$$

With Bernoulli and through a separation of variables in an equation of time and position:

$$w(x,t) = W(x) \times T(t)$$

The equation of position $W(x)$ is resolved into a ordinary differential equation with $\beta$ as the eigenmode:

$$\frac{\delta W^4}{\delta^4 x} - \beta^4 W = 0 \text{ with } \beta = \sqrt[4]{\omega^2 \times \frac{\rho A}{EI}}$$

This formula of position has the general solution:

$$W(x) = A_1 cos\beta x + A_2 sin\beta x + A_3 cosh\beta x + A_4 sinh\beta x.$$

Whereas the solution of the equation of time with $\omega$ as the pulsatance is resolved into:

$$T(t) = A cos\ \omega t + B sin\ \omega t.$$

To determine the constants $A_i$ the solution of the function of position will be inserted in the boundary conditions of the beam. These boundary conditions depend on the fixtures of the beam.

Independently, the solution are four linear, homogeneous equations with coefficients depending on $\beta$. This is the so called eigenwert problem with $\beta$ called eigenwert and its vector $[A_1 A_2 A_3 A_4]^T$. This eigenwert problem can be solved analytical for simple structures with the following function:

$$w(x,t) = W(x)(Acos\omega t + Bsin\omega t).$$

The constants A and B can be determined by inserting the function in the initial conditions $w(x, t = 0)$ for the oscillating displacement and $w'(x, t = 0)$ for the oscillating velocity. After solving the equations for the eigenwerts, the eigenfrequency of the beam is:

$$f_E = \frac{\lambda_F}{2\pi L^2}\sqrt[2]{\frac{EI}{\rho A}}$$

All calculations are only an estimate for the response of a system to a certain impulse. The real initial conditions at a pipe segment are complex and have to be defined in order to compare them to ideal models.

### 2.4.2 Fundamentals of hydraulic oscillation

The resulting displacement movement of the kinematics of the simplex pump exerts a pressure release from the pump's working chamber through the pressure valve. The course and kind of the pressure development depends on the viscosity of the fluid, the working chamber and the pump's quality grade. Depending on the components' characteristics such as valve construction type, opening peak pressures can occur [23]. In consequence they result in impact sound emissions and high-frequency as well as high pressure oscillations, which will be described in the next chapters [26, p. 31].

Looking at an incompressible model (below first eigenfrequency of fluid head), following formulas result with $b_R$ as the fluid acceleration and $v_R$ as the fluid velocity, $b_K$ as the piston acceleration, $v_K$ as the piston velocity, $A_K$ as the piston area and $A_R$ as the inner cross-section area of the pipe [26, p. 38f.]:

$$b_R(\varphi) = b_K(\varphi)\frac{A_K}{A_R}$$

$$v_R(\varphi) = v_K(\varphi)\frac{A_K}{A_R}.$$

Herewith, the pressure losses in the pipeline are time-variable. The acceleration and delay of the fluid mass lead to a change in hydrostatic pressure. This hydrostatic pressure change $\Delta p_M(t)$ is the result of the periodical displacement movement whereas $\rho_{Fl}$ is the fluid density and $L_R$ the pipe length respectively. This quasi-stationary pressure changes can be described as followed [26, p. 39]:

$$\Delta p_M(t) = \rho_{Fl} L_R b_R(t)$$

Friction pressure pulsation occurs at the pipe wall or at the armature through pressure changes as a result of flow loss. For newtonian fluids, these pressure changes can be calculated with $v_R(t)$ as the time-dependent fluid velocity:

$$\Delta p_R = \Big(\frac{\lambda(Re)L_R}{d_i} + \sum_i \zeta_i\Big) \times \frac{v_R^2(t)\rho}{2}$$

As described in all fluid dynamic considerations, it is important whether a turbulent or a laminar current is prevailing. For turbulent currents, the friction pressure losses can be neglected, whereas in laminar currents the flow loss is

$$\lambda_{laminar} = \frac{64\eta}{v_R d_i \rho}$$

At the pump's flange friction and mass pressure changes overlap with a time-variable pressure pulsation evolving:

$$\Delta p(t) = \Delta p_R(t) + \Delta p_M(t)$$

In longer pipelines, the incompressible model is not applicable. Therefore, to characterize the periodical impulse of a pump, the following formula describes the fluid and pipe material depending acoustic velocity $a_{red}$ of a longitudinal wave [47, p. 31] :

$$a_{red} = \frac{a_{frei}}{\sqrt[2]{1 + \frac{E_{fl} d_i}{E_R W_d}}}$$

At discontinuing pipeline points such as bends, pipe ends, changes of intersection and others, reflections of the shockwave influences the continuing course of the shockwave. This leads to an

overlap of back and forth running waves and eventually to big pressure oscillations within the pipe. They are called pressure nodes and anti-nodes.

To calculate the pipe structure with implemented pulsation damper as a compressible model, it can be simplified as a vibration model. The fluid in combination with the elastic pipe wall would be illustrated as the continuum, whereas the displacement pump as the vibration exciter and the pulsation damper as the massless spring. To calculate resonance points of a system and eigenfrequencies, simplifications can be conducted and an approximated maximal pressure amplitude as well as the hydraulic eigenfrequencies can be calculated numerically [26, p. 44 ff].

Magnus et al. stated that after an initial disturbance in an u-bend pipe, the water head oscillates in the u-bend and the occurring oscillations follow a linear differential equation [32, p. 21]. Therefore, it can be stated that even the u-bend itself creates forges and is an actuator in the hydraulic oscillation.

Different methods are available to damp this hydraulic oscillation which leads to high pressure amplitudes and they can be divided into primary and secondary measures. Primary measures reduce the flow rate pulsations while secondary measures reduce the pressure pulsation in pipelines with applications at the pipe system [49]. In most instances economical reasons speak against modifications of the pipeline or deployment of the process engine. Thus, only bezels or pulsation dampers can be considered.

Bezels damp the pressure forges with interference effects whereas pulsation dampers have three impacts: spring-like behaviour in terms of elasticity, dissipating energy through conversion in heat and damping pressure forges through multi reflection [15]. Most dampers are a mixture which damping mechanisms are a combination of the mentioned impacts [26, p. 37].

For a safe operation of the plant it is necessary to calculate the maximum tolerable hydraulic oscillations with the code API 674 developed by the American Petroleum Institute [39][26, p. 57]. All tolerable pressure changes are calculated with $D$ as the outer pipe diameter, $I$ as the area moment of inertia:

$$P_l = \frac{3500}{\sqrt[2]{IDf}}$$

with the tolerable pressure oscillations $f = \frac{(rpm)n}{60}$.

### 2.4.3 Joukowsky and the reflection of forges

In most instances it is easy to prevent the pipeline's extreme loading cases with additional equipment or shelter, whereas the *"Joukowski surge"* is comparable complicated to damp without mounting the pipe or other measures [24, p. 134].

It occurs when a standard check valve in a pump is not closing fast enough. Subsequently a surge is generated because of a back flow building up due to the slow closing valve. This surge can lead to mounting damages, pipe bursting or component damage.

*Allievi and Joukowsky* deduced the following formula at the beginning of the 20th century to describe the surge properly, with $\Delta p$ for pressure difference, $a$ for pressure wave velocity and $\Delta v$ for flow rate: $\Delta p = \rho * a * \Delta v$ [22, p. 246].

Damping the forges is possible with extra applications but hence costly. See chapter 2.3 'Oscillating simplex pumps' and chapter 5.4 'Damping with state of the art applications' for more detail. Regarding friction and mass pressure changes as well as the Joukowsky shocks, the time variable pressure changes are [26, p. 41]:

$$\Delta p(t) = \Delta p_R(t) + \Delta p_M(t) + \Delta p_{Jou}$$

### 2.4.4 Vibrations through pressure pulsation

The transfer of the excitation is transmitted either directly through the displacement pump or indirectly through the fluid head. The direct excitation was discussed before inchapter 2.4.2 'Fundamentals of hydraulic oscillation'. Indirect transfer of vibration with periodic pump oscillation leads to pressure oscillation in the fluid head, which in turn leads to vibration through shaking forces. [26, p. 49ff,70].

The relevant transfer mechanisms are the Poisson effect, friction coupling, impulse force coupling and force through dynamic pressure differences.

The *'Poisson effect'* or pipe breathing includes the radial expansion and contraction of a pipe together with axial lateral contraction. It is negligible in most cases and can lead to a reduction of the pressure amplitude since it dissipates it's energy. The *'Poisson effect'* is partly accounted for in the $a_{red}$ as factor $E_R$.

The second transfer mechanism, friction coupling, is irrelevant for dynamic processes. It describes the friction between the fluid and the pipe wall. With the wall friction depending on the fluid velocity, time-variable axial forces are transmitted to the pipeline. In fact this mechanism is only important in laminar flows [26, p. 51].

As the most important transfer mechanism, impulse force coupling is taking effect on places of the pipe system where the current leads to mechanical impulse forces, e.g. at valves, bends or diameter deviations.

This mechanism has two different physical but synchronized origins: the impulse forces and the dynamic pressure differences result from pressure pulsations. Pipe oscillations generated through these overlapping forces are called shaking forces $F_R$ and depend on the dynamical pressure [26, p. 84f.]

$$F_R \sim \Delta p_{dyn}.$$

The impulse forces originate from the sudden flow rate increase at the beginning of a pressure stage of an oscillating pump. A bend in the pipe system acts as a resistance to the mass flow creating an impulse force $F_i$ with $v_R$ as the fluid velocity:

$$F_i = \dot{m} v_R.$$

The mass flow $\dot{m}$can be replaced with the volume displaced by the piston $\dot{V}$and the flow rate can be replaced with the piston velocity $v_K$:

$$\dot{m}_m = \dot{V}\rho = A_R v_R \rho, v_R = v_K \frac{d_K^2}{d_R^2}$$

This leads to

$$F_i = 0.25\pi v_K^2 \frac{d_K^4}{d_R^2}\rho.$$

After taking the effects of the piston velocity into account and after more calculation steps and with $h_K$ as the piston stroke the impulse force can be expressed as

$$F_i = \pi\rho\eta\Big(\frac{d_K^2 h_K \pi n}{d_R^2 60}\Big)^2.$$

Depending on the distance to the oscillation excitation, the vibration's dynamic decreases over distance since the flow rate is homogenized. In contrary to the dynamic forces resulting

from pressure pulsations, the impulse forces can be neglected in most processing facilities with stream velocities below $2\frac{m}{s}$ [26, p. 86].

Dynamic forces appear because of the time-variable and local distributed pressure pulsations. Especially in bends, they arouse shaking forces and based on direct proportional interconnection between pressure and force, the hydraulic oscillation is transmitted into mechanical oscillation [26, p. 53]:

$$F_{dyn} = p_{dyn} A_R.$$

Crucial for the displacement of the bend is the dynamic pressure ratio which traverses the pipe from point A to B. At $t_0$, only the static pressure exerts at B and $F_{dyn}$ exerts at A.

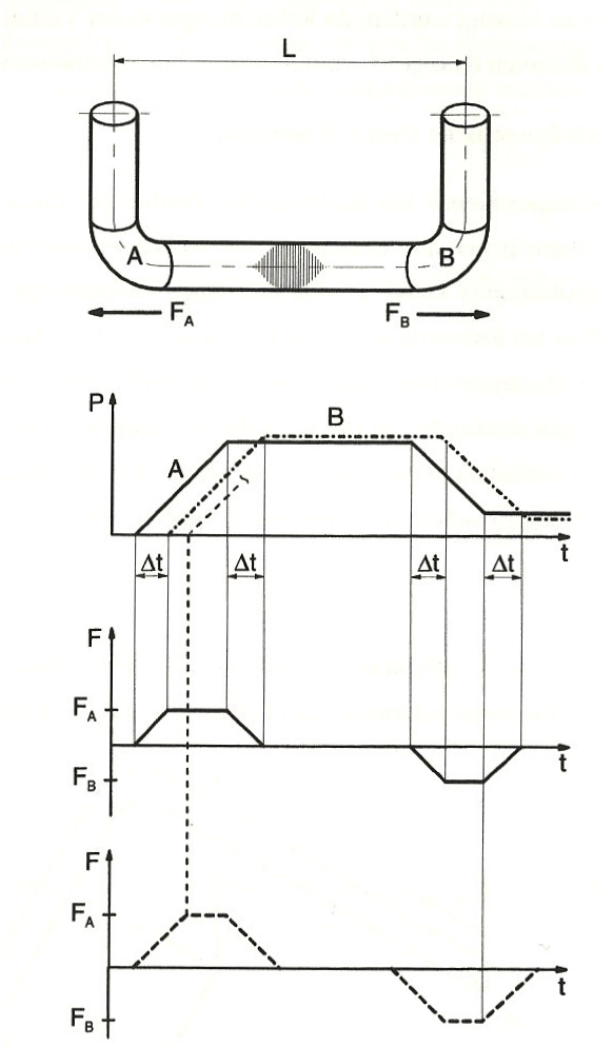


Figure 5: Displacement through pressure pulsation of a pipe (figure taken from [26, p. 54] )

In an u-bend, the force operates at the first bend in the one direction, traverses the straight

part and acts eventually at the second bend in the other direction. Increasing the length of the straight part, the force as well as the timespan between the forces will increase. The difference between these counteracting forces is the absolute value of the shaking force [26, p. 55].

The same is stated by *Tijsseling*: a mounted u-pipe will deform if a dynamic pressure increase traverses the pipe:

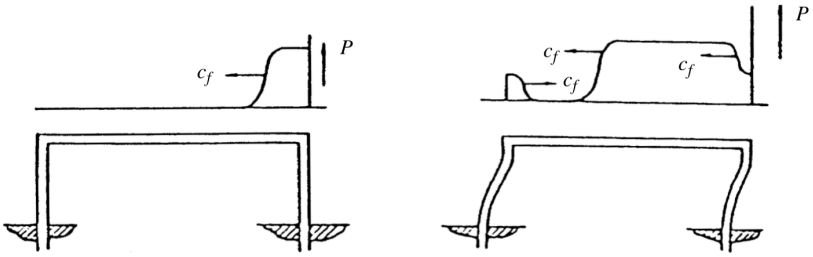


Figure 6: Junction coupling (figure taken from [50, p. 112] )

# 3 Purpose of the bachelor thesis

Granular dampers use *"collective dissipative properties of vibrated granular materials"* to dissolve the kinetic energy of a system. They are passive dampers since they are neither externally actuated nor electrically controlled [45, p. 1]. One of their advantages is the temperature independency and non-degradation over time [5] [25]. They are especially advantageous in comparison to state-of-the-art applications which only have a standard temperature range between -50°Cand +260°C. In areas of energy generation, aircraft and space this characteristic is crucial.

To damp a vibration, they can be applied onto the existing system in the form of boxes, cylinders or other shapes. Another option is to design the structure in such a way that hollow spaces are filled with granular material. The latter requires the design process to precede the structure building and is therefore only applicable to existing structures with destruction or big effort [14, p. 2] [57].

To describe dynamics of particles, two models are most commonly delineated. According to *Li*, they are distinguished by the particle density and the characteristics of the flow that is modeled::

| | *Hard sphere model* | *Soft-particle model* |
|---|---|---|
| Granular flows | Rapid, not dense | Slow, dense |
| Dynamic modeling | Inelastic particle sequencing the conservation of linear and angular momentum | Particles have enduring contacts and/or multi-particle collisions |
| Trajectory simulation | Normal impact: Restitution; for tangential impact: A coefficient of friction | Explicit solution of Newton's equations of motion for every particle at discrete time intervals |

Table 1: Comparison of particle models (information taken from [29, p. 22 ] )

Depending on the basic conditions of the vibration and spacial boundaries, the parameters for the design damper have to be adjusted. The following chapter gives an overview of the fundamentals as well as the different types and previous works on granular dampers.

## 3.1 Theoretical fundamentals

The physical effect of granular dampers is the energy dissipation of inter-colliding particles or particle and wall collisions. [5].

To analyze the effect, granular material was compared to gas particles flowing in a defined two- or three-dimensional space (for example by *Olafsen et al. [36], McNamara et al. [33] or Esipov et al. [17].*

One part of the energy dissipation is the inelastic particle-to-particle collision [19, p. 93 ]. *Esipov et al.* state that the dissipation depends on the restitution $r$ of particles, the particle density $\rho$, the particle size $a$, the system size $L$, and $d$ as the system dimension [17]:

$$1 - r \sim \rho \times L \times a^{d-1}$$

The coefficient of restitution *"characterizes the loss of kinetic energy of the translational motion due to a collision"* [10]. Additional energy dissipation can also occur due to frictional losses [19, p. 93 ] Another part of dissipation is the contact and collision of particles with each other. This happens elastically due to deformation of the particles during collision where *"momentum*

*is exchanged between the structure and the particles, and kinetic energy is converted to heat"* [19, p. 93 ].

The dissipative force between small viscoelastic particles with adhesion is described by *Brilliantov et al.* with both dissipative and adhesive constants and based on the *JKR theory* [27]. However, *Brilliantov et al.* neither covered plastic deformation nor fragmentation. With $R_{eff}$ as a quotient between the product of the particle's radii and the sum of the particle's radii, $A$ as a product of functions depending on the viscous constants, as well as the elastic constants of the particle. In addition is $D$ a parameter of material properties, depending on Young modulus and Poisson ratio, $a$ the radius of the contact area between the particles [10]:

$$F_{dis} = \dot{a}A\left(\frac{3a^2}{DR_{eff}} - \frac{3}{2}\sqrt{\frac{6\pi\gamma}{D}}\sqrt{a}\right)$$

Depending on different parameters of Cluster state description: [34] [28] [13] [12] [58]

The last part of dissipation is the contact and collision of particles with the wall of the observed system. In the fluidized regime *Salueña et al.* found that during a collision with $v \geq \sqrt{Lg}$. $C_g$ being an unknown numerical pre-factor, the velocity $v = A\omega$ and the amplitude $L$, the effective damping parameter $b$ (which is proportional to the ratio between the averaged dissipated power per cycle T and the mean translational kinetic energy of the granular system) is [45]:

$$b = C_g\frac{A\omega}{L}.$$

For velocities $v < \sqrt[2]{Lg}$ the system is only partially fluidized and the dissipated power $b$ equals then, with $C_l$ being an unknown numerical pre-factor [45]:

$$b = C_l\frac{g}{A\omega}.$$

In vibrating granular systems, varying granular damping regimes were observed which also assemble in-between transition phases. With event driven molecular-dynamics simulations, three different regimes were observed by *Salueña et al.* [45] due to different energy losses in a two dimensional system: Solid, gaslike and convective. These regimes have different granular dynamics, therefore the damping efficiency is regime-dependent. *Salueña et al.* described a formula to analyze the effectiveness of a granular setting with $W_{diss}$ as the dissipated power, $T$ as the number of cycles, $m_n$ as the mass and $v_n$ as the velocity of the granular material [45]:

$$b = \frac{\frac{1}{T}\int_T W_{diss}(t)dt}{2\sum_n m_n \int_T v_n^2(t)dt}$$

According to their results, they were able to set up an efficiency diagram with the three regimes included [45].

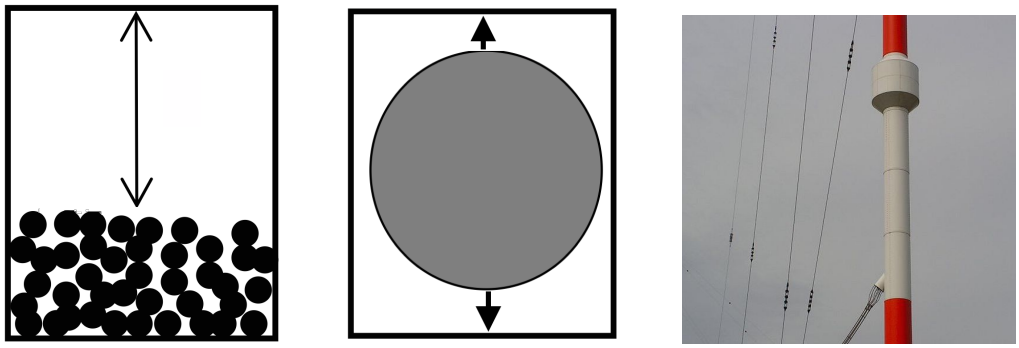

(a) (b) (c)

Figure 7: Particle impact damper (a, (figure taken from [14])), single impact damper (b) and marine transmitter with attached granular cylinder (figure taken from [1] )

## 3.2 Types of granular dampers

Granular dampers can roughly be divided into granular dampers containing multiple spheres, so called particle impact dampers (PIDs, figure 7a) and single impact dampers (SIDs, figure 7b) with only one moving mass per cavity [14, p. 14]. As mentioned before, PIDs and SIDs work in extreme temperature environments if the material of the granulate withstands the temperature. For this reason, steel based granulate materials are favored in most applications. However, using steel granulate both dampers increase the total noise level and the weight at the place of appliance. If low mass or a low noise environment is required, one must take this influence on the design of the damper and the selection of the granulate material into account. To differentiate between these types of dampers a more detailed distinction follows now.

Due to the larger contact area, PIDs create a more equally distributed strain on the container. That leads to less peak load than using SIDs but results in higher surface damage of the inner walls [57, p. 67]. It is also possible to apply a PID in existing hollow parts as for example in spacecraft parts [14, p. 2] instead of applying additional components and decreasing scarce space. If space is not limited, PIDs can also be applied around other structures as in figure 7c.

A PID is a specialized component which is designed to damp a certain combination of frequency and amplitude of displacement [14, p. 15]. There are many applications of with granular dampers but the research on this field has been mainly theoretical and only few studies involve industrial applications. In one application granular dampers are used to damp the most damaging vibrations of transmitter poles to provide a disturbance-free environment for the electronics and signal communications even in heavy weather as in figure 7c [4].

### 3.2.1 Particle dampers

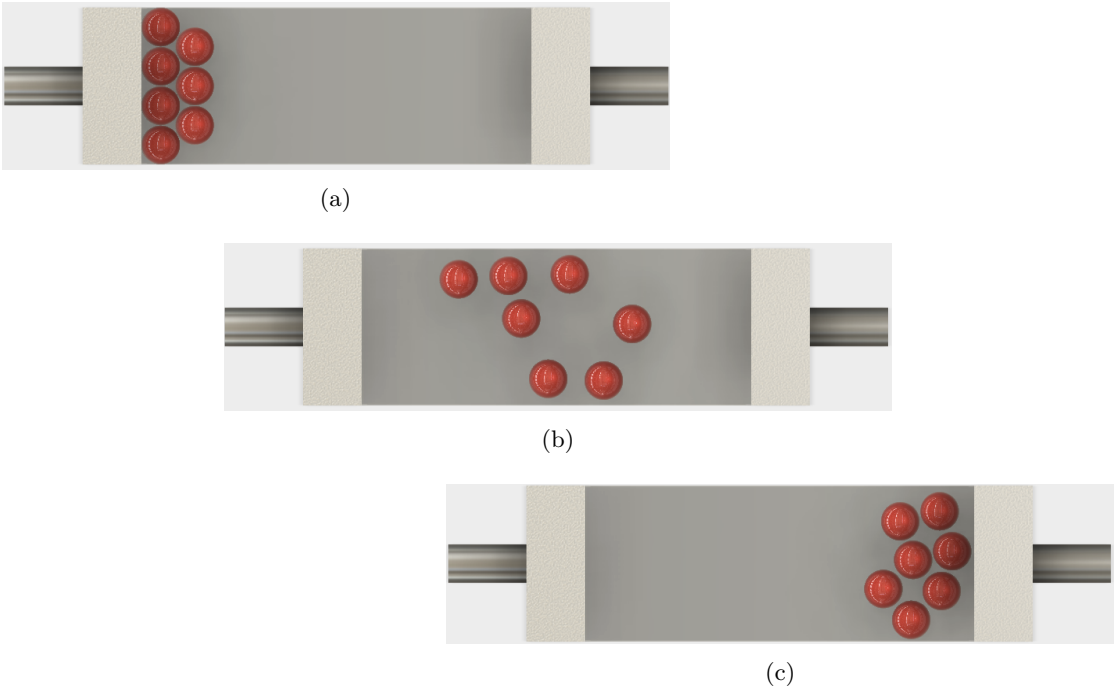

Figure 8: Particle impact damper dynamics; (a) beginning of an oscillation cycle, (b) flying granulate, (c) zero velocity

The dynamical movement of a PID is shown in figure 8a-c. In figure 8a, the acceleration of the granulate is given by the box, in figure 8b, the energy is mostly kinetic and in figure 8c all energy has been dissipated by the collision. Most energy is dissipated at the walls with particles colliding with the walls perpendicular to the direction of oscillation.

Previous work on impact dampers was done for example by *Ramachandran et al.* [40]. Their work underlines the importance of predicting the effectiveness of PIDs with different parameters using numerical methods. They conclude that two-impacts-per-cycle solutions should be considered for an effective damper design.

*Lu et al.* studied a particle damper and it's effects on a three story steel frame structure that was excited at its bottom with free vibration, random excitation and an onsite earthquake excitation. Under these conditions they found that a buffered particle damper can effectively damp building structures [30].

*Marhadi and Kinra* concluded that a more precise model of PIDs should involve the size and particle as parameters and describe them as a cluster instead of single particles citeMarhadi2005.

*Yang* analyzed the effectiveness of PIDs. After long runs he found that an abrasion coating builds on the granulate's surface which decreases the damper's effectiveness [57, p. 30 ]. In addition, he found that the dissipated power in a PID does not change with higher particle sizes but equal mass [57, p. 67].

### 3.2.2 Single impact dampers

*Papalou and Masri* compared the efficiency of SIDs with PIDs. They concluded that SIDs are more effective for damping one frequency with an achieved maximum vibration attenuation of around 80%. Nevertheless, the sound emissions of PIDs are lower then those of SIDs and they have a vibration attenuation between 60 and 70% while having a broader damping frequency spectrum. They investigated a horizontally vibrating single-degree-of-freedom system under random base excitation. Finally they set up an optimum design of particle dampers under a certain frequency, range and box length [38].

### 3.2.3 Multi unit and combined dampers

An insight in the effects of multi-unit particle dampers was given by *Saeki*. These dampers consist of more than one cavity containing granular material. Their findings show a connection between the mass ratio (total mass of granular particles divided by the mass of the primary system) and damping efficiency. The optimum cavity damper is achieved with a cavity radius decrease for every additional cavity [44].

*Du and Wang* analyzed the impacts of a fine particle impact damper where the inner box of the damper is coated with elastic particles and a single bigger sphere is placed inside the box (see figure 9. The plastic deformation of the fine particles used is important for the energy dissipation. For a low frequency domain, the fine particle impact damper's performance is much better than those of SIDs [16, p. 1015].

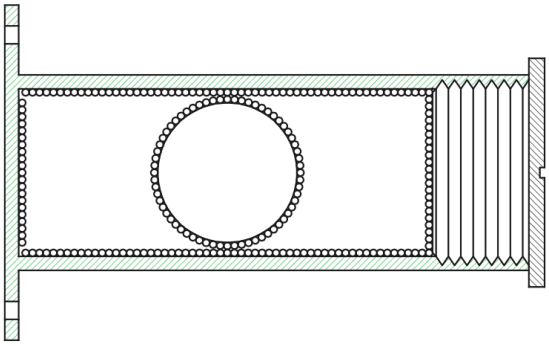

Figure 9: Fine particle impact damper schematics (figure taken from [16, p. 1016] )

## 3.3 Design principles

Many approaches to design an effective damper have been undertaken ([6] [42][57][41][55][19][30]) and they all studied parameters that influence the damping of the setting.

> *"The design problem is compounded by the large number of design parameters, such as the geometry of the enclosure, the material of the particles, the shape of the particles, the packing configuration of the particles, and the application of the field of force around the particles [55]."*

With this work it is attempted to imply all the mentioned publications and design a damper for an industrial application. Two of the most important parameters are the box length as well as the mass of the inserted granulate.

# 4 Experimental setup

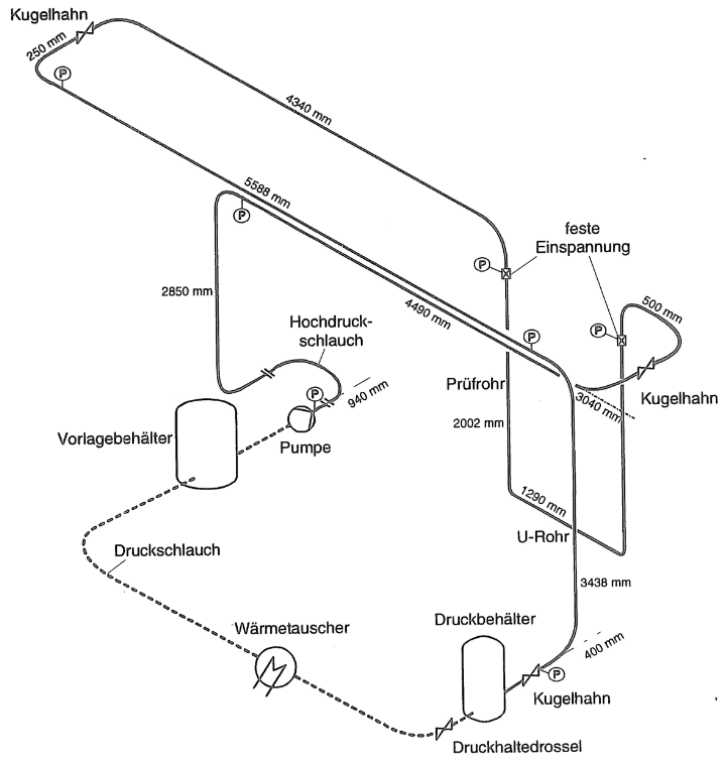


Figure 10: Schematics of the pipe system (figure taken from [26, p. 93] )

In 2002, *Dr. Dietmar Jarmer* analyzed the mechanical excitation of pipe vibrations with oscillating displacement pumps in the context of his dissertation [26]. To achieve this, he used a numerical calculation and verified it consequently with experiments at the technical center of the IPAT chair (Lehrstuhl für Prozessmaschinen und Anlagentechnik) of the Friedrich-Alexander-University of Erlangen-Nuremberg.

The experimental setup consists of a water tank, where water as the working fluid is stored. A valve pump (pulsation generator) pumps it from there through a high-pressure hose and around a 28m long pipe where the main focus of the experiment is fixed: a u-shaped pipe. The water goes through a pressure holding throttle valve, an optional bladder accumulator (to reduce the amplitudes of pressure oscillations), a heat exchanger, and a pressure container (see figure 10). Optionally the water can be lead in a loop.

The following chapter will describe his setup and findings about the vibrations of the u-shaped pipe which can be found in industrial facilities as described in chapter 2.2 'U-bend expansion joint'.

## 4.1 Piping - old setting

| **Pipes** | |
|---|---|
| Manufacturing technique | Seamless drawn, scale free |
| Material | Steel 1.4571 |
| Dimension | 30 x 2.5 |
| Outer diameter | 30 ± 0.08mm |
| Inner(nominal) diameter | 25 ± 0.08mm |
| **Fitting** | |
| Manufacturer | Ermeto |
| Kind | Progressive ring fitting |
| Material | Steel 1.4571 |
| Class | S (heavy) |
| Nominal diameter | 25mm |
| Strength | PN400 |
| **Gear** | |
| Manufacturer | SAWA |
| Type | SN 160 RV |
| Transfer ratio | 3.55 : 1 |

Table 2: Pipe data sheet (table taken from[26, p. 94])

Special attention was paid at adjusting the setting in a way that the mechanical eigenfrequencies of the u-pipe in-plane (x-y plane, see figure **??** ) as well as out-of-plane (x-z plane) are within the excitation range of the pump. This was done by oscillation calculations of the pipe. The surrounding frame is fixed to the ground and the walls. The inner pipe diameter is 25mm, the pipe is made out of stainless steel and more specifications give an overview of the used components and dimensions in table 2.

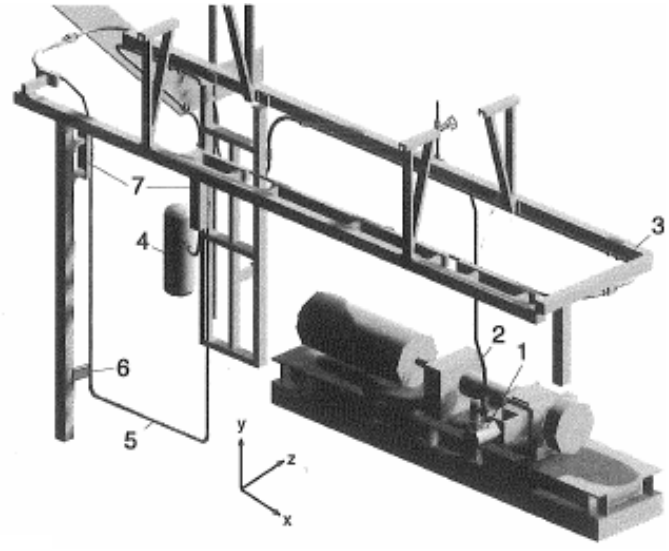


Figure 11: Pipe system schematics (figure taken from [26, p. 95,89])

*Dr. Jarmer* lead the working fluid water in a closed loop and prevented it from heating with a heat exchanger (see figure **??** ).

The u-bend is mounted only on top of the pipe system as visualized in figure 10 as number 7. This prevents the y-directional movement of the u-bend [26, p. 132ff]. The bend radius of the inserted u-pipe was knowingly chosen small to force big shaking forces [26, p. 94].

## 4.2 Modifications for this work

To measure the motion of the pipe only one laser displacement measuring device was applied in x-direction (see figure **??** ) instead of two as described in chapter 4.4 'Measurement devices'. In addition to the former described setup in chapter 4.1 'Piping - Old setting' (see Figure 10) a pipe u-bend on the top was changed to a straight pipe run and the following pipe guidance was designed to suppress the movement of pipe in z-direction. It uses two in the floor rigidly mounted stands with rolls wich can rotate due to ball-bearings. Furthermore, the four white rolls in figure 12 are made out of Teflon® for less friction.

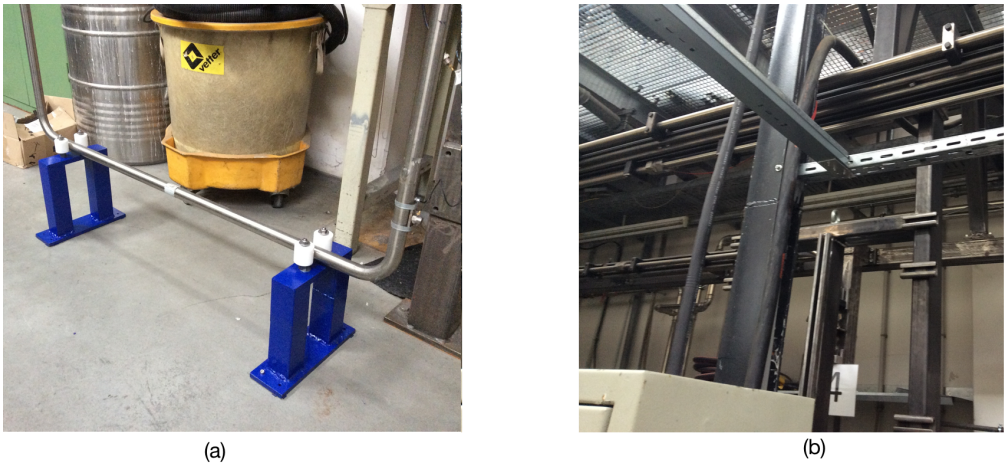

(a) (b)

Figure 12: Laser sensor, channeling (a) and straight pipe run (b)

## 4.3 Pump

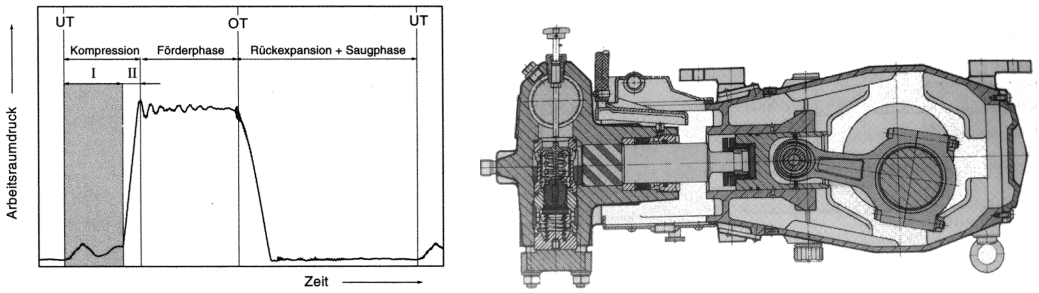


(a) (b) Structure of a simplex pump

Figure 13: (a) Generated pump pressure; (b) structure of the simplex pump (figure taken from [26, p. 92, 3]

The general function of a simplex pump is described in chapter 2.3 'Oscillating simplex pumps'. The utilized pump (LEWA LS-1) has a quasi-harmonic straight thrust crank gear.

To test the system with different volumetric degrees of efficiency, *Dr. Jarmer* mounted an adapter to adjust the elasticity of the working chamber and therefore a change in the degree of efficiency up to 30% which was not used in this thesis and left at around 98%. The setting was designed with a flexible high-pressure hose in front of the pump (see figure 10) so that no vibrations of the pump, the motor or the driving mechanism are transferred to the pipe system. The following data sheet of the pump system components describes their specifications.

| **Pump** | |
|---|---|
| Manufacturer | LEWA |
| Type | LS-1 |
| Displacement | Piston |
| Number of pistons | 1 |
| Driving mechanism | Linear surge crank drive |
| Driving rod Ratio $\lambda_S$ | 0.187 |
| Piston displacement $h_K$ | 45 mm |
| Piston diameter $d_K$ | 30 mm |
| Maximum delivery pressure | 100 bar |
| Range of rounds per minute | 60 ... 600 $min^{-1}$ |
| Volumetric efficiency $n_V$ | max. 98% |
| Valve type | Convex cone valve |
| Valve nominal diameter DN | 32 mm |

| **Motor** | |
|---|---|
| Manufacturer | Anton Piller |
| Type | KLA 834-4 |
| Engine output P | 2.3-45 kW |
| Range of $n$ $[in\ min^{-1}]$ | 120-2400 $min^{-1}$ |

| **Gear** | |
|---|---|
| Manufacturer | SAWA |
| Type | SN 160 RV |
| Transfer ratio | 3.55 : 1 |
| | |

Table 3: Data sheet of the pump (table taken from [26, p.90] )

## 4.4 Measurement devices

To analyze the system, *Dr. Jarmer* added pressure (all sensors in or after the pump), bending stress (at the top of the u-bend), acceleration and displacement (bottom of the u-bend), flow and temperature (before and after the pump and u-pipe respectively) sensors to the system as shown in figure 14. This opened the opportunity to measure all hydraulic and mechanical influences and changes.

*Dr. Jarmer* chose a sampling rate of 5 kHz to measure and analyze fluid sound velocities and pipe accelerations with a frequency of >100 Hz [26, p. 108]. For the new requirements of analyzing the displacement a sampling rate of 1 kHz was chosen since a smaller rate leads to an imprecise result as shown in figure **??** 'data measuring points'. In addition the runtime of the data analysis is more applicable with 1 kHz than for higher sample rates.

| Measured variable | Sensor description | Manufacturer | Device type | Measuring range |
|---|---|---|---|---|
| Working chamber pressure $P_A$ and pipe pressure $P_{5,6}$ | Pressure sensor, piezo-resistive | Keller | PA-15-200 | 0 - 200 bar |
| Pressure $P_{1-4}$ | Pressure sensor, piezo-resistive | Kistler Instrument AG | 4045A200 | 0 - 200 bar |
| Pressure $P_7$, $P_{Reservoir}$ | Pressure sensor, piezo-resistive | Keller | PA-15-400 | 0 - 400 bar |
| Pipe acceleration $a_{x1} - a_{z2}$ | Acceleration sensor, piezo-electric | Bruel & Kjaer | 4367 | 0 - 20 kHz |
| Pipe displacement $s_{x1}, s_{z1}$ | Laser triangulation sensor | Micro-Epsilon Messtechnik GmbH& Co KG | LD1605-200, LD1600-50 | $\pm$200 mm, $\pm$50 mm |
| Bending stress $\sigma_{1,2}$ | Strain gauge | HBM | - | - |
| Piston stroke length $h_k$ | Displacement sensor, inductive | HBM | W50 | $\pm 50mm$ |
| Angle of revolution $\phi$ | Encoder | Heidenhain | ROD 451 | 3600 Imp./r. |
| Flow rate $\dot{V}$ | Flow control unit | $E + HFlowtex$ | Picomag II | - |
| Temperature | Thermocouple | Braun Messtechnik GmbH | NiCr/Ni | - |

Table 4: Measurement devices data sheet (table taken from [26, p.97] )

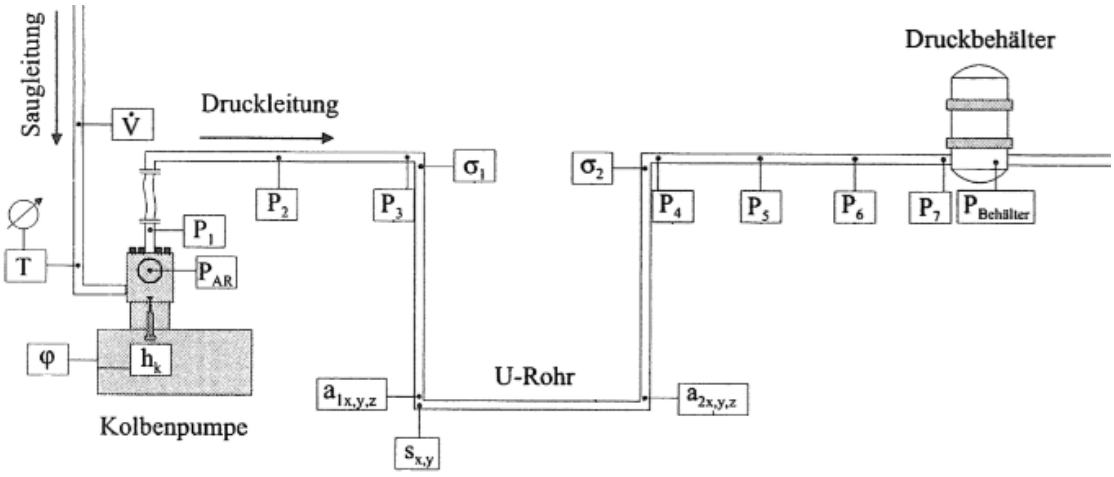


Figure 14: Schematics of the measurement devices (figure taken from [26, p. 96] )

# 5 Previous work

This section aims to present the results of *Dr. Jarmer* in a way which is necessary for the fundamental understanding of the system and previous results of the occurring vibration.

As shown previously in chapter 4.4 'Measurement devices', there are a number of sensors applied to the system. Figure 15 shows an extract of how a typical data set looks like. In figure 14 'Measure schematics', you can see the different measuring points of the sensors. The pump pressure determines the hydraulic oscillations (middle of figure 15) of the system as it can be seen for example between 0.35 and 0.45 s. Here the working space pressure $P_A$ affects $P_1 - P_5$. Also the mechanical sensors measure affects of the pressure peaks (bottom of figure 15).

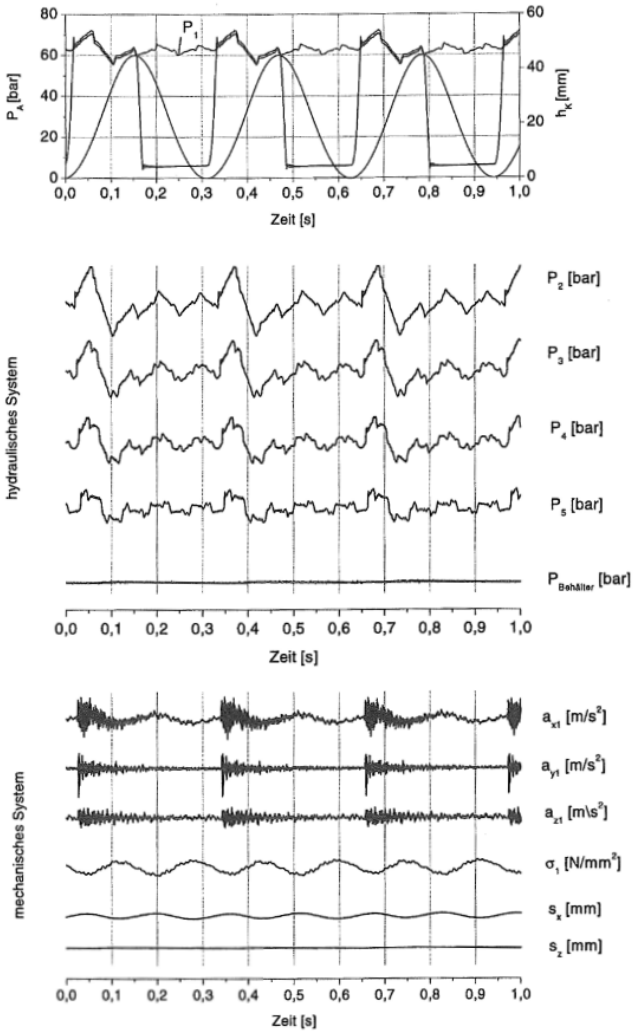


Figure 15: Signal example from *Dr. Jarmer* at 190 $min^{-1}$ and $p_F = 60bar$(figure taken from [26, p. 114] )

## 5.1 Hydraulic oscillation

The pump's stroke displacement consequently leads to pipe pressure oscillations and a fluctuating flux in the pipe. In figure 16a is the pressure in the pump's working chamber whereas the rows of figure 16b show the different pressure sensor positions P1-P6. With increasing position in the pipe the amplitude is decreasing. See left column in figure 16b where the amplitude is steadily decreasing from P1 to P6. This is due to energy losses through expansion of the pipe as well as leaks of the pipe connections.

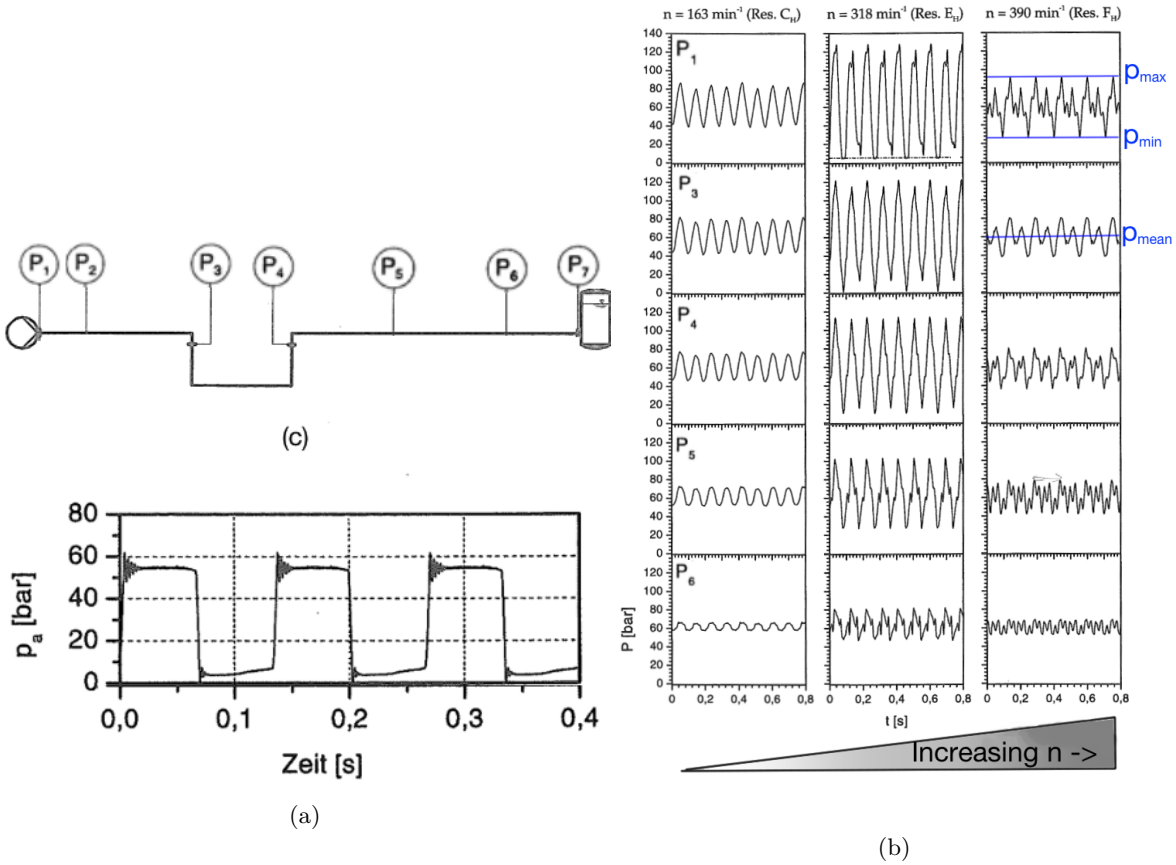


Figure 16: Pressure-time-diagram of different measure points (figure taken from [26, p. 120,98] )

The mean pressure (right column of figure 16b) of the system is regulated by the pressure throttle (see bottom right of figure 10) [26, p. 88]. This is an important adjustment parameter for the oscillations as well as the later described vibrations. Furthermore, the amplitude is nonlinearly depending on the pump's revolutions per minute $n[inmin^{-1}]$. This can be observed in figure 16b where $n$ in the first column is 163, in the second 318 and in the third 390. Even though the $n$ is increasing, the amplitude is decreasing from the second to the third column. Additional frequencies for increasing $n$ can also be observed in figure 16b.

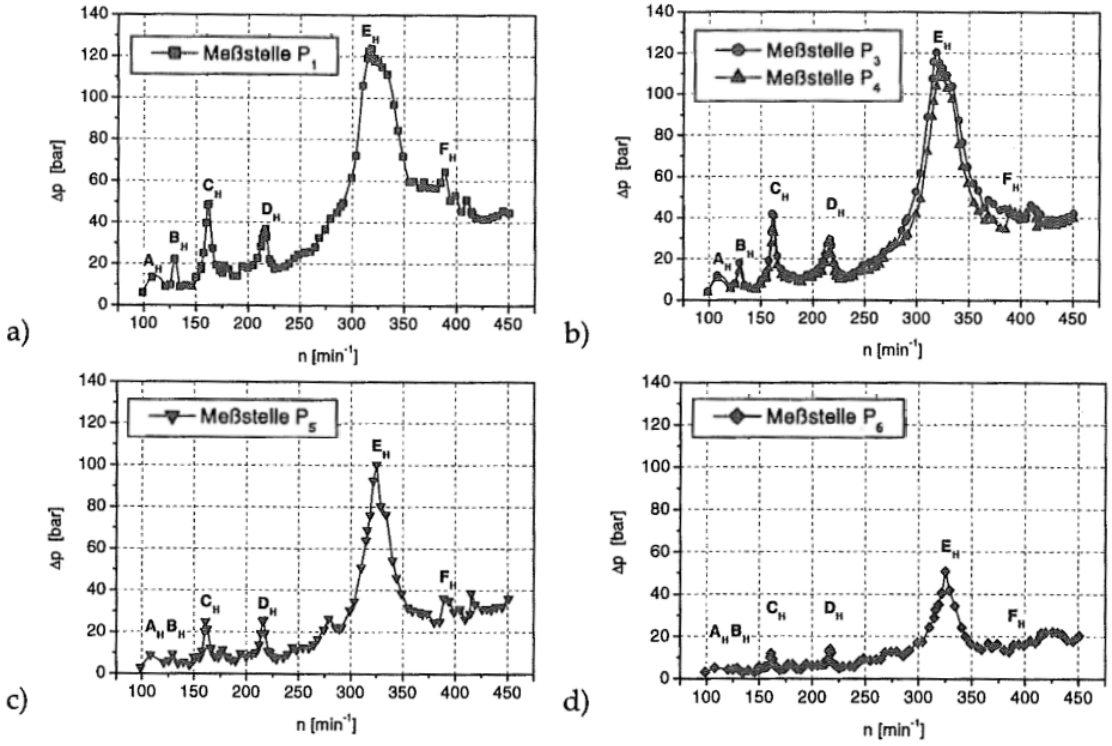


Figure 17: Pressure pulsations at different positions as indicated in figure 16c (figure taken from [26, p. 118] )

The x-axis of figure 17a is the pumping frequency in $min^{-1}$ and the y-axis are pressure fluctuations. They are defined by $\Delta p = p_{max} - p_{min}$ (see figure 16b, right column) and are nearly constant at different measuring points as it can be seen in the figure 17. The resonance peaks do not depend on the position within the pipe (compare figure 17 a-d). For example in both figures 17a and c, the peak $E_H$ is around n=325$min^{-1}$. The major hydraulic peaks have been labeled A-F and with index H for hydraulic.

The occurring hydro-acoustic resonance frequencies were at 11.02Hz and 33.06Hz respectively and they were expressed in 3-9 times the pumping frequency [26, p. 119].

He concluded that the local pressure amplitude distribution is frequency-dependent. From a hydroacoustic viewpoint, due to two pressure antinodes and nodes it is a closed-open system.

See figure **??** with pipe schematics and chapter 4.1 'Old setting' for information on how the space coordinates and the overall set-up are defined.

## 5.2 Hydraulic and mechanical comparison

The pressure gradient at P3 and P4 (see figure 16c) is an important parameter for the shaking forces in the u-pipe [26, p. 117]. Figure 17b shows the difference of both at different $n$.

In regard to figure 18 where the x-axis is the pumping frequency in $min^{-1}$ for all plots and the y-axis in the first plot is the $\Delta p$ of P3. The second plot shows the acceleration difference in $m/s^2$ and the third the displacement difference in $mm$. There is no direct dependency of resonance points of hydraulic oscillation and mechanical vibration since no peaks of the pressure are matching either the acceleration (middle plot) or the displacement. The peaks of the displacement and pressure are not correlating in the $n$ [$in\ min^{-1}$]spectrum. For example, the highest hydraulic peak $E_H$ is at around 320 $min^{-1}$ whereas the highest mechanical peak $C_M$ is at 350 $min^{-1}$.

An interpretation of figure 18 shows that the most important data is:

- the size of displacement since it leads to system damage
- $A_m$ *and* $C_m$ are highest existing peaks
- highest mechanical peaks are in x-direction

Therefore, the following work will focus on damping the peaks at $A_m$ ($n \approx 175\,min^{-1}$) and $C_m$ ($n \approx 350\,min^{-1}$). The frequency of $A_m$ in both cases is a multiple of 5.8 Hz hence one of the mechanical eigenfrequencies of the system.

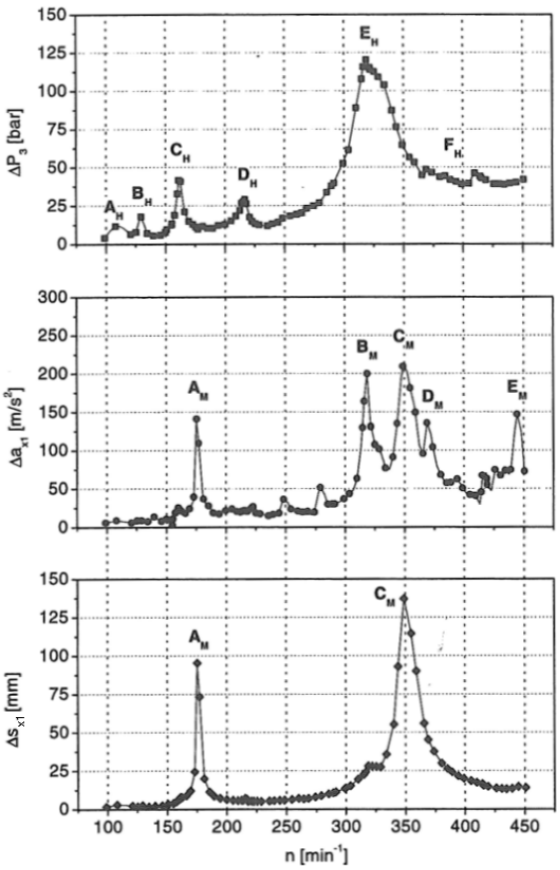


Figure 18: Comparison between hydraulic an mechanical behaviour (figure taken from [26, p. 139] )

## 5.3 Mechanical vibration

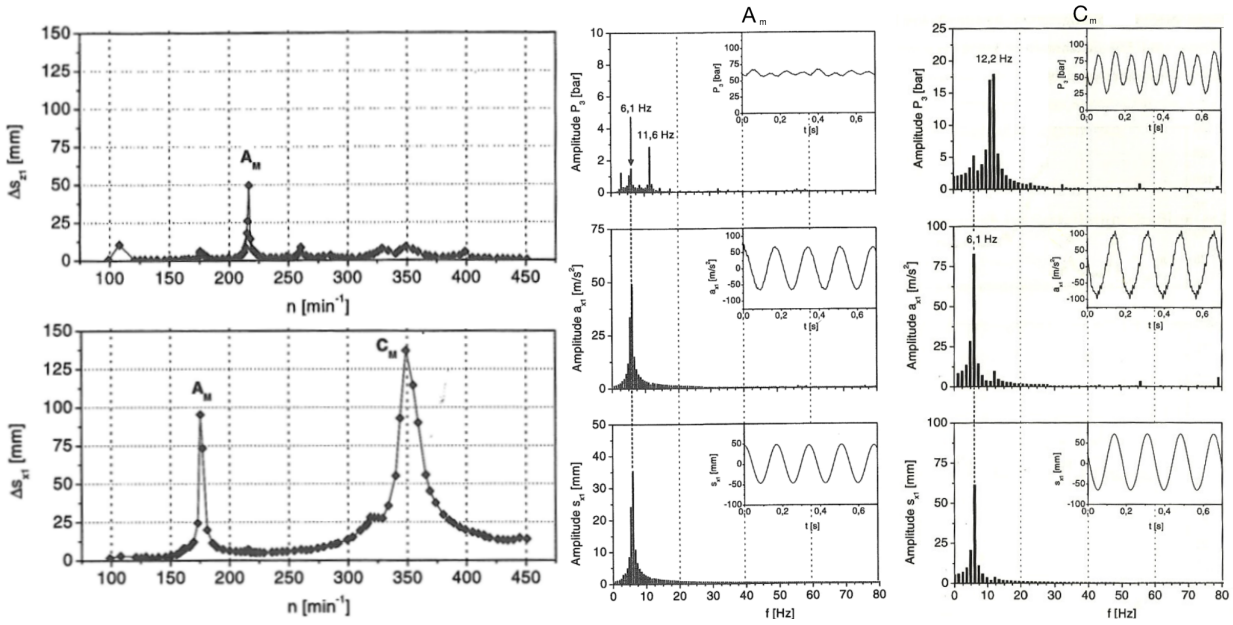


(a) (b)

Figure 19: Diagrams of the resonance points $A_m$ and $C_m$ (figure taken from [26, p. 139, 141, 145f.]

In figure 19a the displacement amplitude of the pipe vibration are shown over the pumping frequency. The top figure shows the displacement in z-direction (out of the u-pipe plane) and the bottom figure shows the amplitude in x-direction (in-plane). Since the displacement and acceleration in z-direction is not as significant as in the x-direction (see figure 19a, where $A_m$ and $C_m$ in x-direction are higher than $A_m$ in z-direction), it will be suppressed for this thesis.

From the results of *Dr. Jarmer*, the conclusion can be drawn that no direct correlation between acceleration in x and z direction exists. The most significant two peaks are $A_m$ at $175 min^{-1}$ with $\Delta$s=95mm and $C_m$ at 350 $min^{-1}$ and $\Delta$s=137mm. The spectral analysis of these two peaks are shown in figure 19b and both show a peak of $s_x$ at 6.1Hz.

## 5.4 State of the art dampers

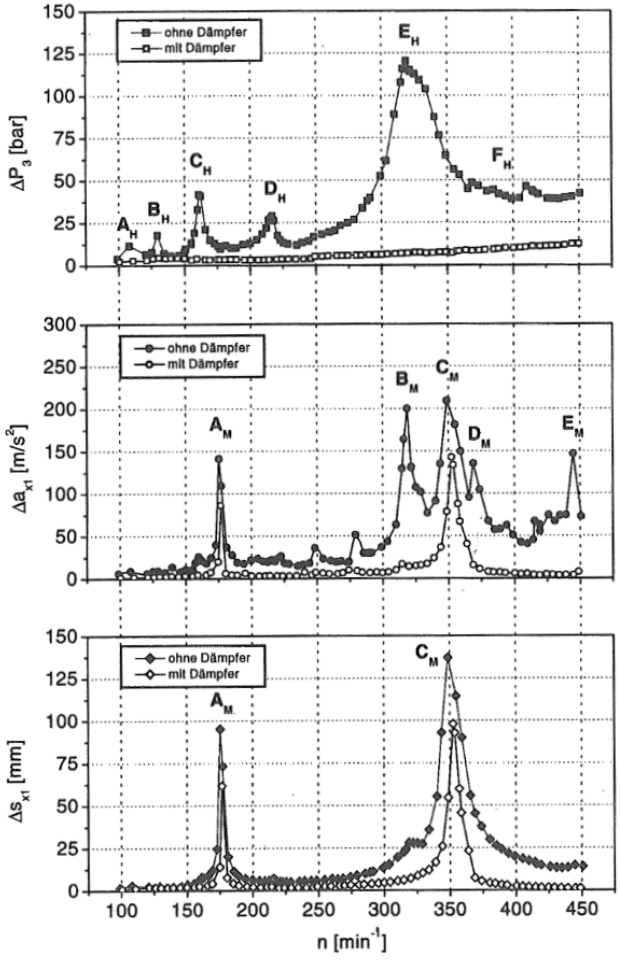


Figure 20: Influence of a gas damper on the system (figure taken from [26, p. 159] )

Hydraulic pulsations can be damped with gas dampers as described in the subsection 2.3 about compressed air dampers. After applying gas dampers hydraulic eigenfrequencies are moved to lower, less dangerous levels. This can be observed in the top of figure 20, where the normal hydraulic oscillation is shown and the hydraulic oscillations after applying a gas damper (white circles).

However, applying a gas damper works well in z-direction and damps all peaks to an acceptable level. But the resonance points of the pump are still evoking high x-direction displacements at the points $A_m$ and $C_m$ (see figure 20, bottom graph) [26, p. 157ff]. Hence the damping of the displacement in x-direction is the single focus of this thesis and lead to a modification of the setup as seen in chapter 4.2 'Modifications for this work'.

# 6 Results

The aim of this thesis is to analyze the application of a granular damper to damp the mechanical oscillations of a vibrating pipe of the existing experiment with additional applied components. The damping does not lead to a linear decay of the amplitude as shown by *Bannerman et al.* [6] or *Sack et al.*[42] since the pump and pipe structure which steadily induces forces onto the u-pipe. Instead the amplitude of the oscillation is permanently decreased.

Firstly the boundary conditions must be clarified. One constraint is that the pump should not run much higher than $300n$ $[in\ min^{-1}]$due to high load on the system [26, p. 147]. Another constraint is that the damper can only be applied on the horizontal part of the u-pipe to provide for a symmetric setting and the possibility to adjust the length of the damper at the position where the maximum amplitude occurs. The horizontal part of the u-pipe has an overall length of 1290 mm and additionally the channelling is minimizing this length to around 1000 mm (see figure 10 'schematics of pipe run').

As mentioned before in chapter 5.3 'Mechanical vibration' the damping in x-direction with a granular damper is the goal of this thesis. The biggest peaks were identified at $A_m$ and $C_m$ which have to be verified again with the newly applied components. The goal will be achieved with different settings of the damper further described along this chapter.

## 6.1 Design of the damper

### 6.1.1 Implementation of design principles

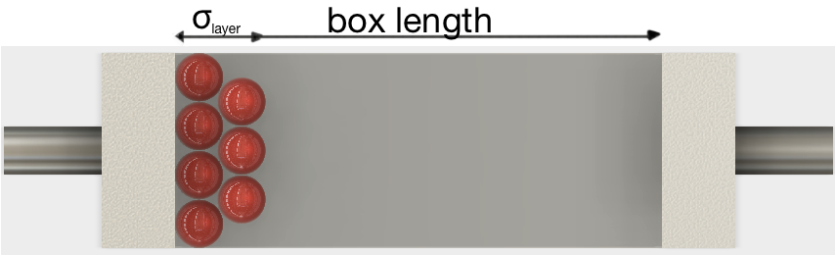


Figure 21: Definition of $\sigma_{layer}$ and box length

In 2011, *Bannerman et al.* set up a formula to describe the most efficient box length of dampers in microgravity, with $A_0$ as the amplitude of the vibration, $M$ as the container's net weight, $N * m$ as the total mass of the inserted granulate and $\sigma_{layer}$ as the thickness of the granulate layer when packed on a surface (see figure 21)[6, p. 6]:

$$L_{opt} = \pi A_0 \sqrt{\frac{M}{M + Nm}} + \sigma_{layer}$$

Even though the pipe experiment is under normal gravity conditions the maximum length of the box was ascertained from this formula since the pipe length is limited (due to adjustment requirement of box length).

The oscillating mass is also the u-pipe filled with water, which is about 16kg. This influences the $L_{opt}$ in a way that it equals around 300 mm (with an $A_0 = 68.5\ mm$ and $\Delta s_x(C_m) = 2 * A_0 \approx 137\ mm$ ). Due to the mentioned restrictions and an oscillation impeding through the channeling and the mass of the damper filled with granulate, the author chose a maximum damper length of around 200 mm.

Various studies set up design principles and procedures for granular dampers (for example [18], [37], [31]). Resultant as an important adjustment of the damper is the box length and the mass of the granulate which is defined by $\sigma_{layer}$.

### 6.1.2 Design requirements

The following damper design requirements need to be fulfilled to achieve sound and reproducible results:

- The granular dynamics need to be observable
- The inner box needs to be variable in size
- Withstanding all occurring forces and endure long experimental runs
- No additional kinetic interaction with the system
- The mounting on the pipe withstands all forces and doesn't weaken the pipe or blocks the flux
- The inner box walls should withstand the kinetic forces and, like all materials, be rust-proof

### 6.1.3 Final damper design

All mentioned parameters were taken into account in the damper design and in conjunction with Michael Miller of the 'Mechanikwerkstatt der Technischen Fakultät der FAU Erlangen-Nürnberg', the author designed the damper as follows using *PTC® Creo 2.0* CAD software:

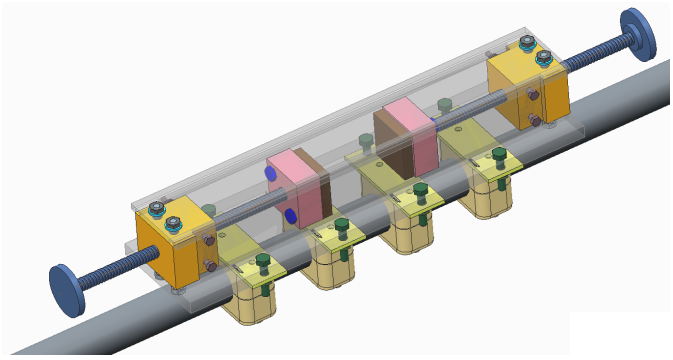

Figure 22: Granular damper design

To have the possibility to observe the dynamic of the granulate, PMMA plastic was selected as wall material of the damper container (transparent grey walls in figure 22). In the first step, the walls were glued together. Since the granulate is steel spheres, the transparency of the walls might only be influenced if, as a result of high impact forces, the spheres produce steel dust particles. These might lead to scrapers on the PMMA, but for this experiment it was decided that the PMMA walls are sufficient for the above mentioned requirements.

Stainless steel threaded bars were used to adjust the box length precisely and variable to the extend of the length of the container (long threaded dark blue parts in figure 22).

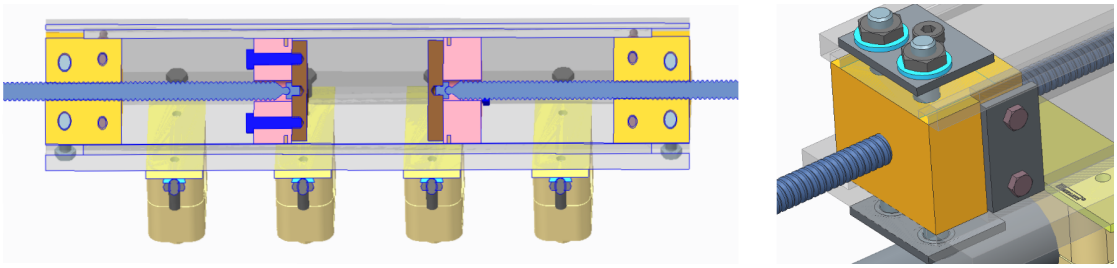

Figure 23: Cross section and detail view of granular damper

The symmetry of the damper was essential to prevent unwanted kinetic interaction with the system. Stainless steel plates absorb the kinetic energy to ensure longevity of the damper (dark brown parts in figure 23). Four clamping pieces (light yellow parts in figure 23) ensured on the one hand that the damper is mounted safely and on the other hand the prevention of pipe damage during operation.

To warrant that the box length can be adjusted smoothly, Teflon® plates were screwed in place behind the metal plates (pink parts in figure 23) which have an inserted felt slice to forestall dust from coming between the Teflon® and the PMMA walls. The fixture walls (yellow parts in figure 23) were made out of aluminium and screws were used to fix the PMMA walls together with glue to ensure that the granulate can be changed with opening one side of the damper. Finally, addressing concerns that the PMMA might get cracks as a result of vibrations, additional stainless steel plates were designed to dispense the peak surface pressure at the screw holes (dark grey parts in detail view of figure 23).

The final damper is shown in figurefigure 24.

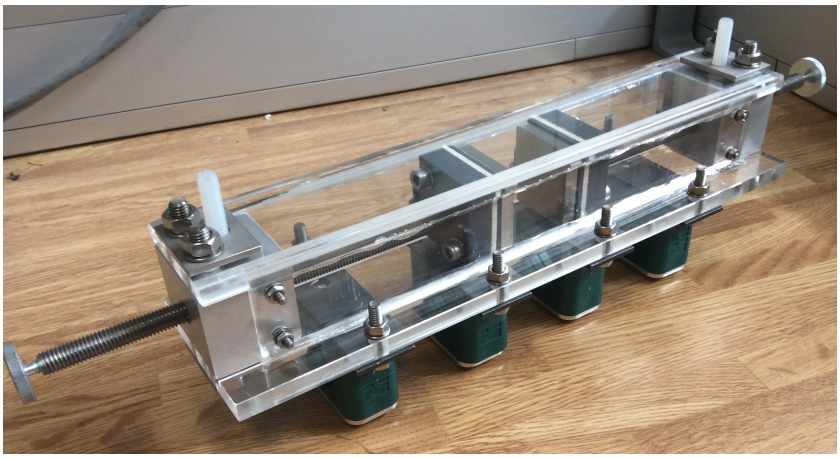

Figure 24: Final damper design

The next page shows figure 25: the technical drawing of the final design and it's dimensions. A total weight of the damper was measured at 2,480g.

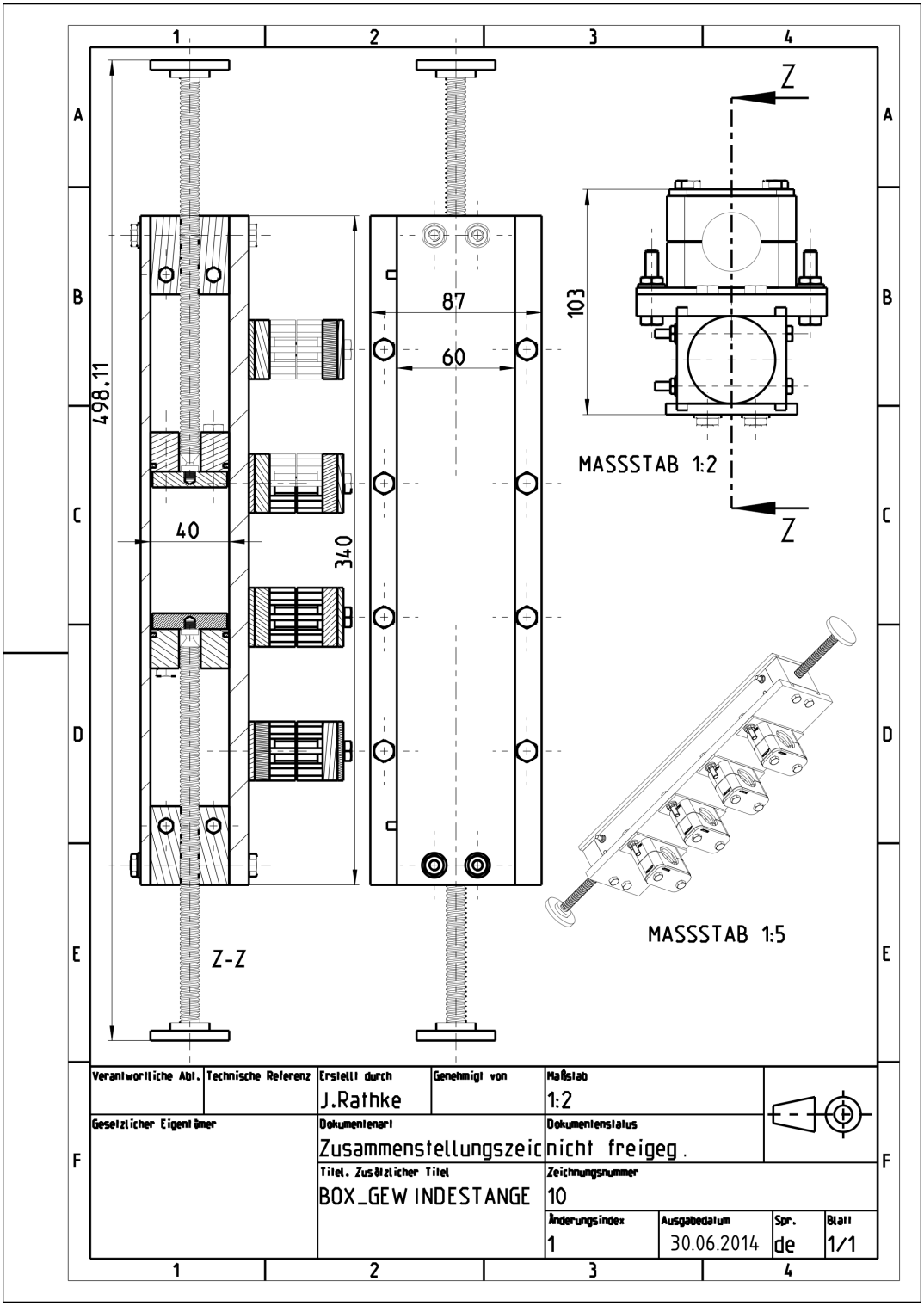


Figure 25: Final design CAD drawing

## 6.2 Investigated system parameters

Before analyzing data of the experiment it is necessary to analyze which sampling rate is required for the purpose of analyzing the displacement of the pipe. Different sampling rates ranging from 50-1,000 Hz are shown in figure 26. Above 1,000 Hz is not reasonable since it is more than the twentyfold of the maximal occurring frequency in the setting (which in this experiment is 50 Hz) and increases the computational effort [26, p. 108] [8]. The author chose 1,000 Hz to be able to analyze the pressure and acceleration accurately in case of problems occurring within the pump or pipe system.

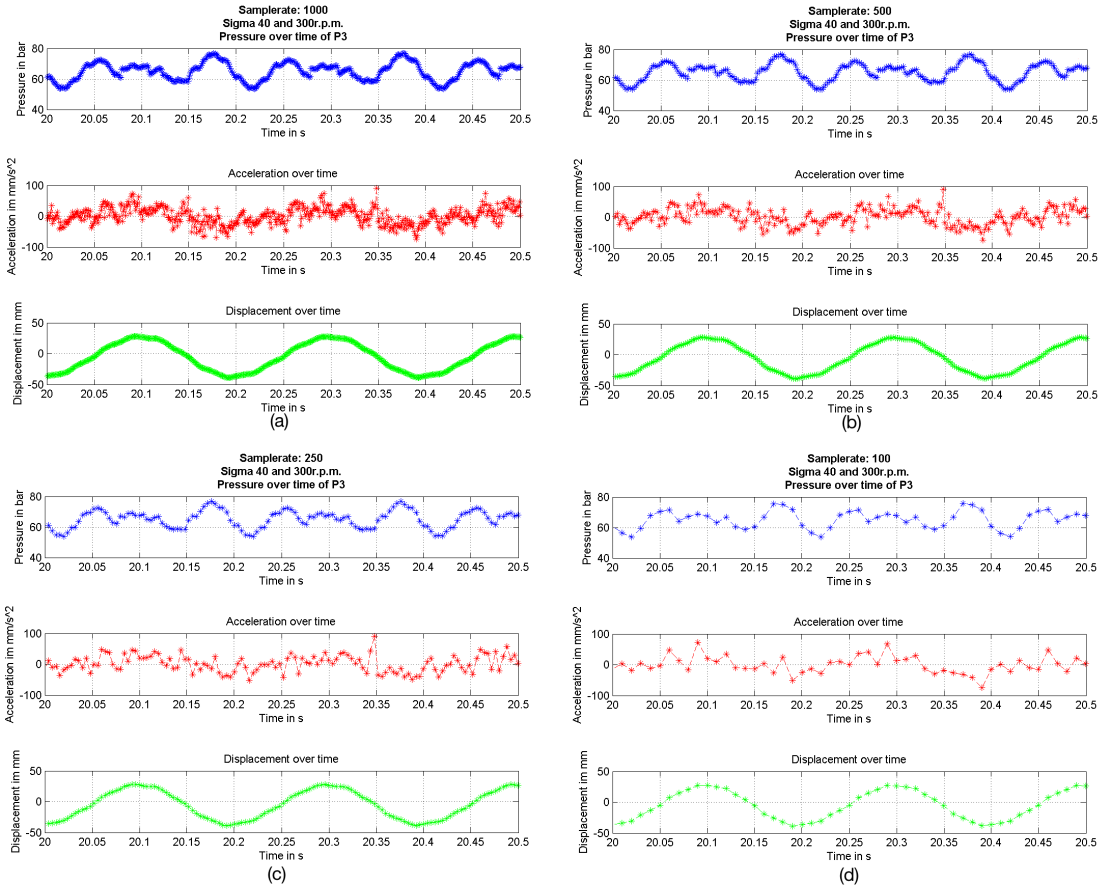


Figure 26: Different sample rates of the same setting: $\sigma_{layer} = 40\ mm$ , 300 $n[inmin^{-1}]$

In figure 26, four different sample rates over time are shown. In figure 26a, a data sampling of 1000 Hz is shown with the pressure in bar in blue, the acceleration $mm/s^2$ in red and the displacement $mm$ in green. The other sample rates are 500 Hz (figure 26b), 250 Hz (figure 26c) and 100 Hz (figure 26d) As seen in chapter 5.3 'Mechanical vibration', *Dr. Jarmer* analyzed a scan of the displacement in comparison to the $n[inmin^{-1}]$. The previous section stated the highest peaks were *"$A_m$ and $C_m$ which have to be verified again with the newly applied components"*. The author repeated a $n$ $[in\ min^{-1}]$scan and retrieved the following data:

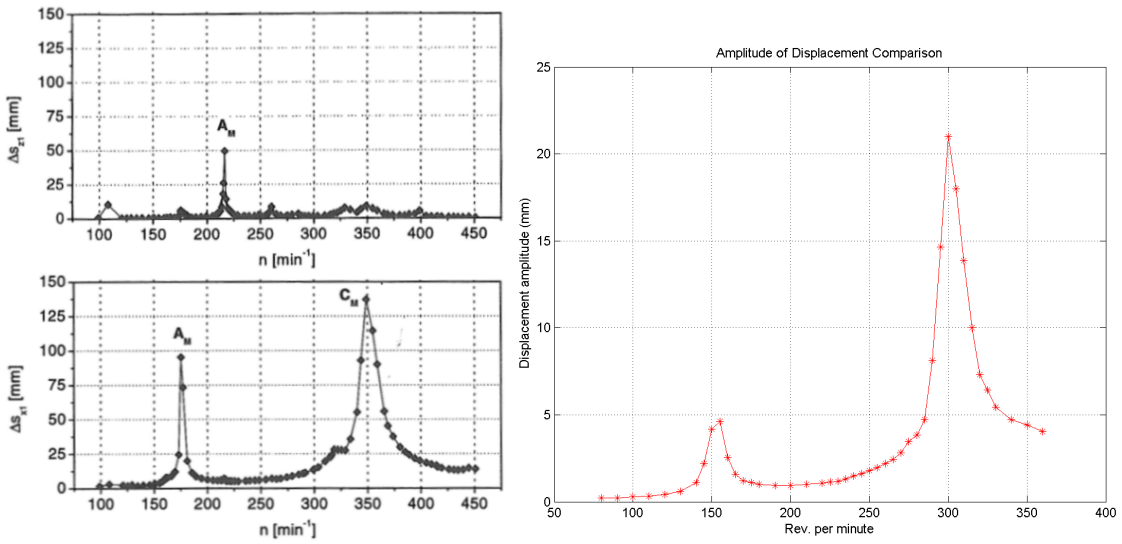


(a) (b)

Figure 27: Displacement $n$ $[in\ min^{-1}]$scan without a damper (figure (a) taken from [26, p. 139]) and with new appliances (b)

In figure 27a an old data set is presented, showing the displacement (in $mm$)in z-direction on top and in x-direction on the bottom over the pump frequency (in $min^{-1}$). The new displacement scan with an empty box mounted on the u-pipe and the channeling applied as described in chapter 4.2 'Modifications for this work' can be seen in figure 27b. This answers the question at which $n$ $[in\ min^{-1}]$the most measurements should run: 300 $n$ $[in\ min^{-1}]$since the system shows the highest displacement with the empty damper and with a channeling at this $n[inmin^{-1}]$. Another advantage to choose 300 $n$ $[in\ min^{-1}]$is operation safety (see beginning of chapter 6 'Results').

In chapter 6.1.1 'Implementation of design principles' and chapter 3.1 'Theoretical fundamentals', the author demonstrated a few damping parameters.

In the following chapters, an analysis of the following system parameters at 300 $n$ $[in\ min^{-1}]$is presented:

- Box length of the damper
- $\sigma_{layer}$ as the thickness of the granulate layer when packed
- Jammed granulate (ergo $\sigma_{layer} = box\ length$)

## 6.3 Reference measurements

The influences of dynamical and jammed granulate were investigated and in the following the gathered data is illustrated exemplary for $\sigma_{layer} = 50\ mm$ :

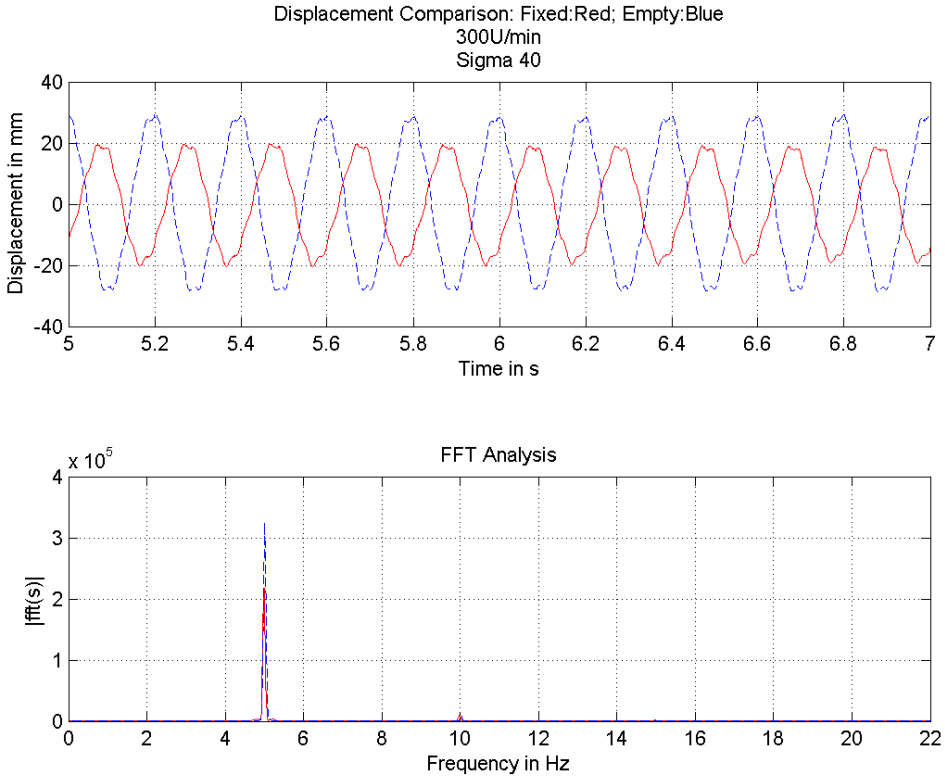


Figure 28: Amplitude of displacement, blue equates the jammed setting, red equates a box length of 85mm

A change of amplitude can be observed in figure 28, where (in the top figure) displacement over time is shown. The blue graph shows an empty damper which has a higher amplitude than the red one which shows jammed granulate. The frequency of the displacement also changes. In figure 28 on the bottom, the jammed granulate (red) has not a higher frequency than the empty damper and both have a frequency of around 5 Hz. This led to further investigation of the parameters. The results are presented in the following chapters.

## 6.4 Influence of the damper application and other parameters

### 6.4.1 Weight of granulate

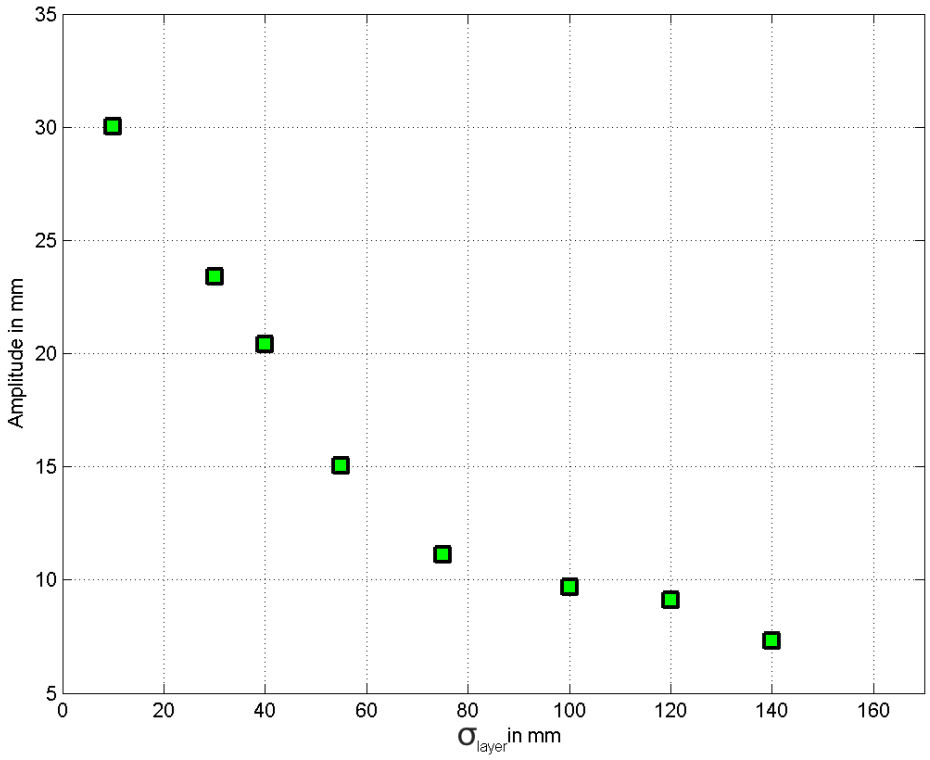


Figure 29: This figure shows the mass damping (y-axis is displacement in mm) at 300 $n[inmin^{-1}]$ of different $\sigma_{layer}$ (x-axis)

In figure 29, the amplitude of the displacement is shown over the $\sigma_{layer}$. The green squares represent the displacement of jammed granulate. With small $\sigma_{layer}$ a higher amplitude reduction is possible with dynamic damping because the vibration amplitude is significant in comparison to higher $\sigma_{layer}$. The damper application influences the system also as follows: Applying weight on the u-pipe decreases it's displacement and acceleration hence the shaking forces stay equal whereas the accelerated weight increases. Pressure or flux changes were not observed and are not influenced significantly by inserting more granulate.

A test was set up to analyze how the weight of the damper with different $\sigma_{layer}$ variations. The results are presented below:

### 6.4.2 Boxlength

Changing the box length at 300 $n$ $[in\ min^{-1}]$influences displacement as observed in figure 30. Here, the example at $\sigma_{layer} = 40\ mm$ with the amplitude (in mm) over the box length (in mm) is showing the damping and reinforcing regime:

| $\sigma_{layer}(in\ mm)$ | *10* | *30* | *40* | *55* | *75* | *100* | *120* | *140* |
|---|---|---|---|---|---|---|---|---|
| **First trial** | 2583 | 2751 | 2830 | 2937 | 3101 | 3297 | 3452 | 3603 |
| **Second trial** | 2546 | 2731 | 2793 | 2936 | 3040 | 3271 | 3375 | 3539 |
| **Third trial** | 2590 | 2745 | 2819 | 2944 | 3107 | 3291 | 3437 | 3608 |
| **Average** | 2573 | 2742.33 | 2814 | 2939 | 3082.66 | 3286.33 | 3421.33 | 3583.33 |

Table 5: Weight measurements in grams of different $\sigma_{layer}$ with damper

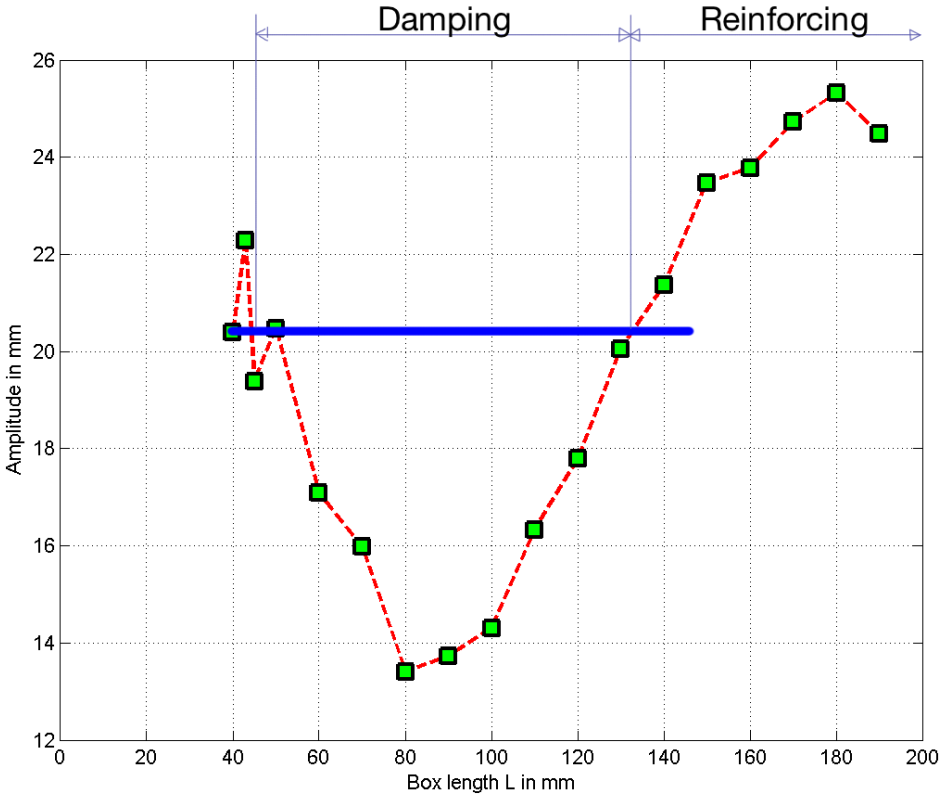


Figure 30: Run of the displacement curve of $\sigma_{layer} = 40\ mm$ over different box lengths. Above the blue line, the granulate box acts as a vibration reinforcer and below as a damper.

The same analysis was repeated for different $\sigma_{layer}$. In figure 31, the starting point of each curve equates jammed spheres ($\sigma_{layer} = box\ length$). For example a $\sigma_{layer}$ (or layer height) of 10 mm is jammed at a box length of 10 mm. The x-axis is again the box length and the y-axis represents the displacement amplitude.

The closer analysis of figure 31 leads to a few interpretations which are illustrated as following:

- There occurs also negative damping or accelerated vibrations (over green dashed line of $\sigma_{layer} = 55mm$ figure 31). The starting displacement amplitude is smaller than the amplitude at higher box lengths (shown with dashed line).

- The negative efficiency might be connected to different damping regimes. In figure 31 $\sigma_{layer}$ which stay below or equal the starting displacement amplitude can be seen.
- There is an overall effective damping trend in figure 31 (read opac area) and an inserted mass which will lead to only negative damping ($\sigma_{layer} = 140\ mm$ only reinforces the vibration).

As seen by *Saeki* in 2002, the mass ratio ($= \frac{weight\ granulate}{weight\ vibrating\ system}$) influences the damping significantly [43, p.159f.]. However, his work was mainly about small weight changes and a reinforced displacement was not exposed as it can be seen in figure 31.

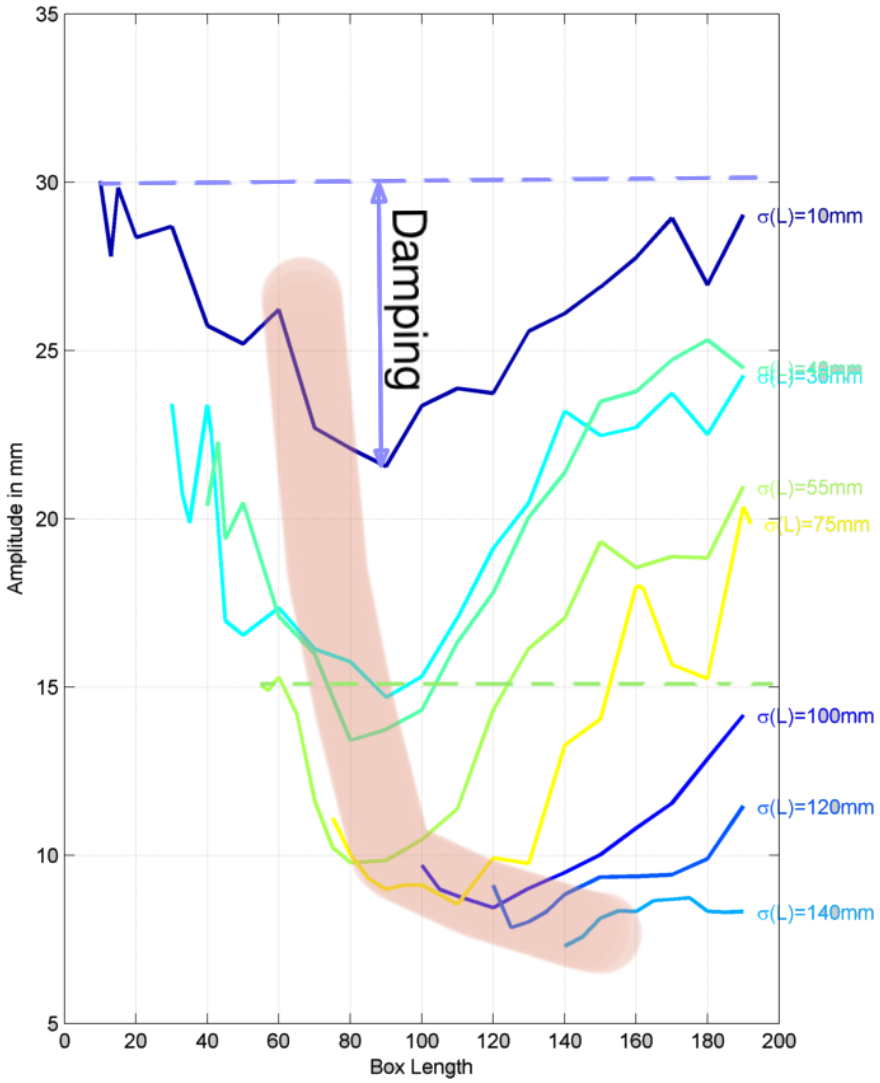


Figure 31: Amplitude of displacement comparison between different $\sigma_{layer}$ and box lengths

### 6.4.3 Particle diameter

Changing the particle diameter also effects the damping behavior but was not part of this thesis and might be part of future experiments with a similar setting. This was one of the results for example by *Saeki* [43, p.160].

## 6.5 Overview of damper optimization

The last part of the analysis concentrates on damping efficiency for the setting described in chapter 4.2 'New setting'. The following filling fraction will be used:

$$Filling\ fraction = \frac{\sigma_{layer}}{Box\ length}$$

The efficiency of this setting is furthermore defined as:

$$Damping\ efficiency = 1 - \frac{Current\ displacement\ (with\ box\ length > \sigma_{layer})}{Displacement\ of\ fixed\ \sigma_{layer}}$$

Firstly the question to be investigated was at which $\sigma_{layer}$ the highest damping efficiencies occur and how they differ from each other. Figure 32 shows the maximum damping efficiency of different $\sigma_{layer}$.

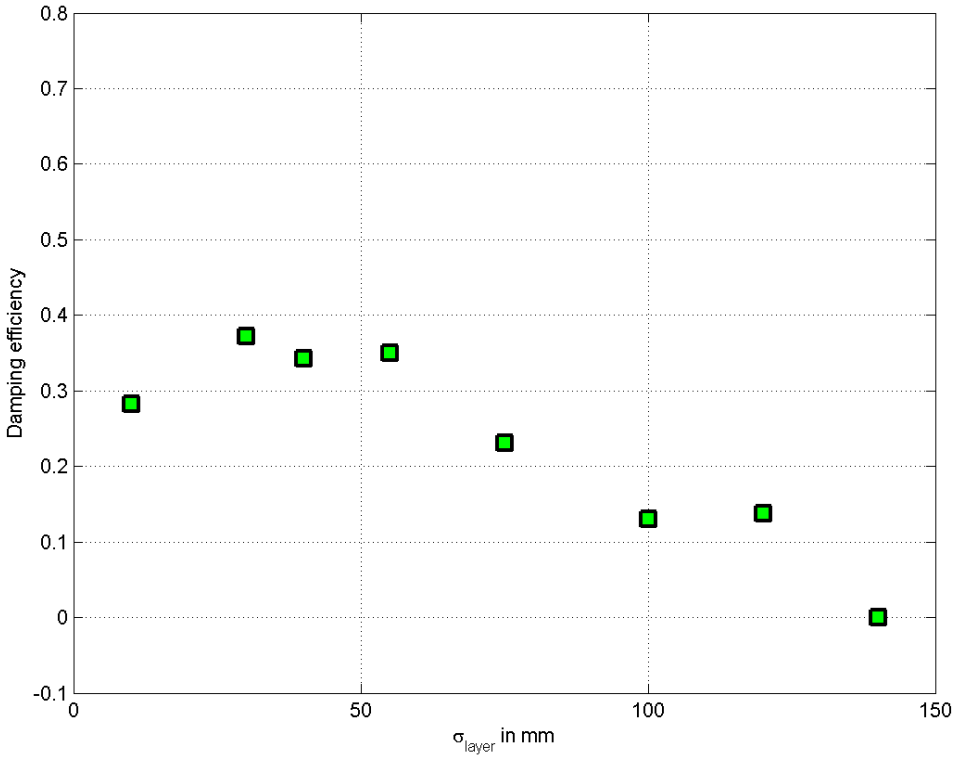


Figure 32: Maxmimum damping efficiency of different $\sigma_{layer}$

A slight but not a significant downward trend can be seen in figure 32. On the other hand with figure 33 showing the absolute displacement (compared to jammed granulate) of the different $\sigma_{layer}$, there is a clear trend towards reinforcing the vibration with a higher $\sigma_{layer}$. This means that a damping is also possible for small $\sigma_{layer}$. This is important for lightweight design applications and if the available space is limited.

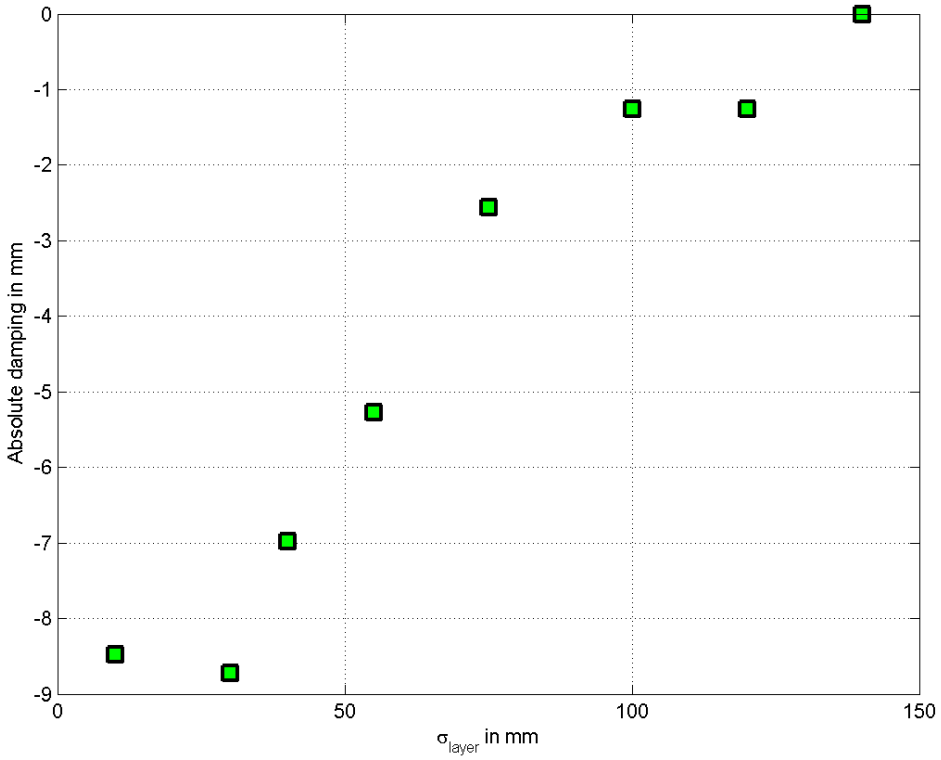


Figure 33: Absolute displacement efficiency

To have a rough overview of the damping spots and how the damping efficiency, filling fraction and $\sigma_{layer}$ are associated, a 3D plot was created which includes all parameters (but due to different means of data analysis, the efficiencies can not compared to the figures shown before):

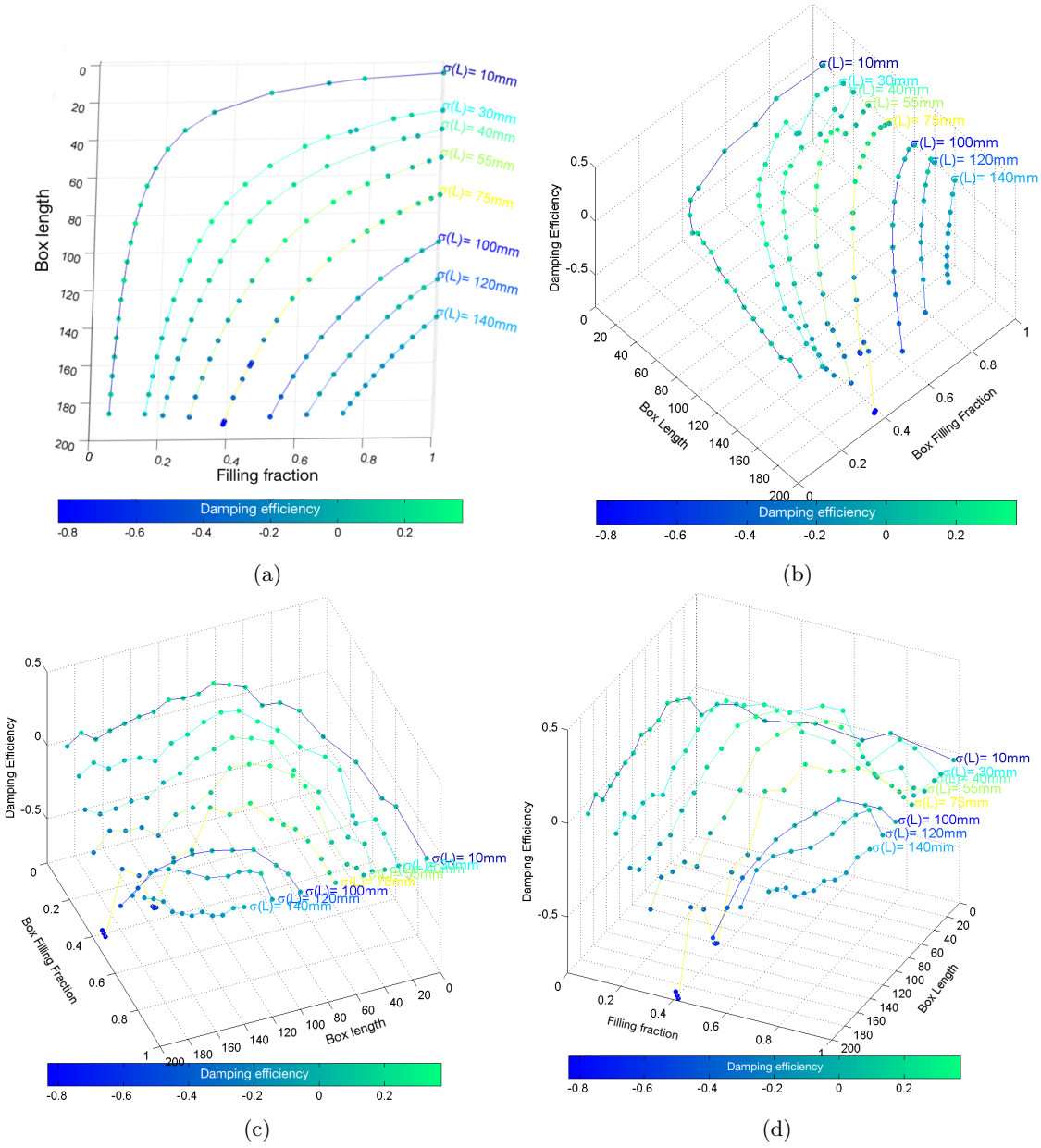


Figure 34: 3D damping efficiency: the dot's color indicates efficiency, box length in mm. These plots only give an idea of the damping spots and do not represent the same efficiency as shown before since the method of analysis differs to previous shown figures.

In figure 34 the reader can see the parameters filling fraction, box length and damping efficiency (dot's color indicates efficiency) and the different line colors specify the different $\sigma_{layer}$. An area of efficient damping can be spotted which is approximately at a filling fraction of 0.4 to 0.6 and a box length of 60 to 100 mm. Also areas of inefficient or negative damping can be spotted, mostly at high box lengths. Furthermore, to mark the areas more clearly a different color scale was used and the spots were sketched generously. A 2D representation of the filling fraction

over the box length with a contour color scale showing a rough sketch where the damping spots approximately can be spotted in figure 35 (but again, due to different means of data analysis, the efficiencies can not compared to the figures shown before):

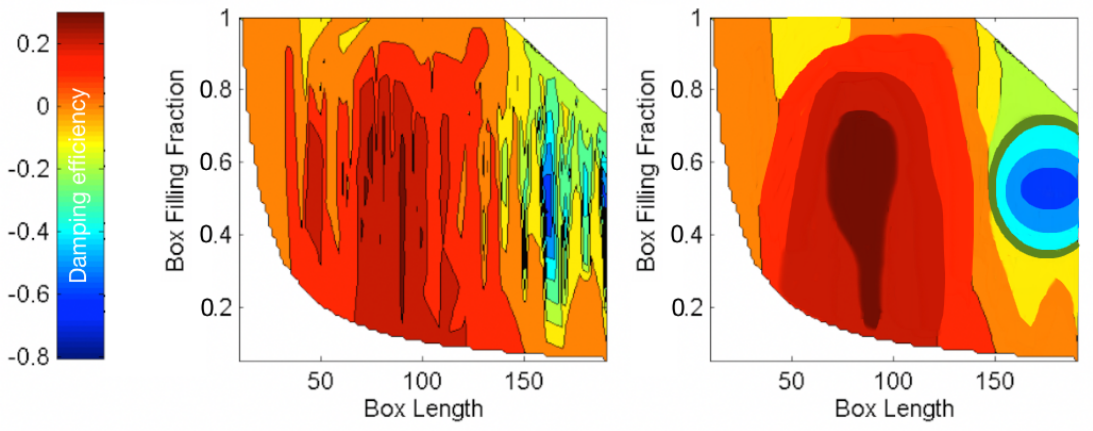


Figure 35: Contour plot of efficiency. Left: Detailed spots, right: sketched spots. These plots only give an idea of the damping spots and do not represent the same efficiency as shown before since the method of analysis differs to previous shown figures.

Using this information of an efficient damper application on this pipe system the subsequent upcoming question was: how does the efficiency change if granulate is placed into the damper first with the box jammed and then with a filling fraction of 0.5 (taken from the maximum efficiency, see figure 35). The result is shown in the following diagram, where the y-axis is the displacement amplitude in mm and the x-axis are pumping frequency $n$ (note: the efficiency difference to figure 35 can be explained by an preceding pump adjustment).

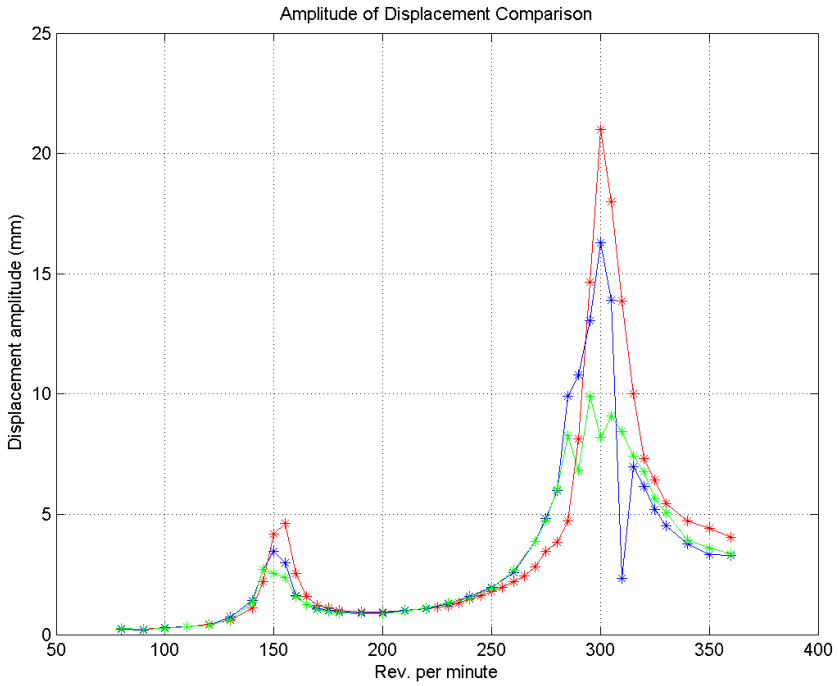


Figure 36: Variation of the damper at a $n$ $[in\ min^{-1}]$scan; red: Empty damper, blue: $box\ length = \sigma_{layer} = 40mm$ (jammed), green: $box\ length = 80mm$, $\sigma_{layer} = 40mm$

Snapshots of the dynamic granulate were captured at different $n$ $[in\ min^{-1}]$in figure 37a-d:

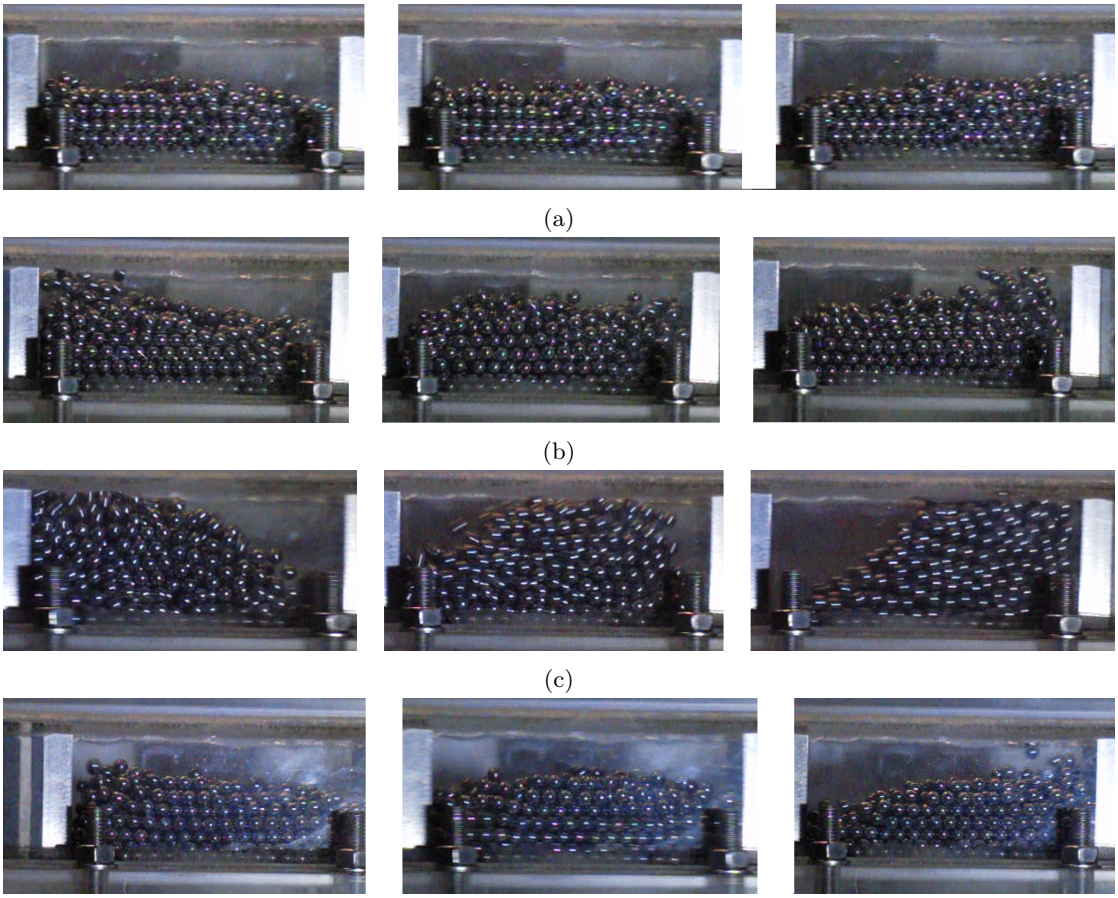

Figure 37: High-speed dynamic glance of (a) 280 $n[inmin^{-1}]$, (b) 290 $n[inmin^{-1}]$, (c) 305 $n[inmin^{-1}]$, (d) 320 $n[inmin^{-1}]$

In figure 37a and 37b the granulate is not accelerated it only 'billows' like a small wave from wall to wall. Around 300 $n$ $[in\ min^{-1}]$the granulate is dynamic and moves like a cluster from wall to wall. After the peak, the granulate decelerates again into the wave-like state (see figure 37d).

# 7 Outlook: future granular damper applications and designs

Possible damper applications are very widespread and do not need any power supply. They dissipate the power through kinetic energy dispersion with granular materials, preferably steel.

In this thesis it was shown that although the industrial system boundaries are complex it is possible to successfully apply a damper. Moreover close to 40% dynamic damping (compared to jammed granulate) was achieved with the initial damper design, without the secondary mass damping. Furthermore, the vibration frequency of the system is not disturbed. The loading forces are damped but the vibration frequency stays equal to the previous vibration frequency. That means that an industrial design is not influenced by applying a granular damper to it. This allows engineers to analyze existing vibration problems and develop granular damper that damp the vibration effectively. As a result, many vibration problems could be counteracted in the early lifetime of chemical plants and even consumer products. The lifetime could be extended and the maintenance reduced.

Further research and development in this area may redundantize other dampers or heavy dimensioning of vibrating structures and industrial products.

Many of the previous research was set up to damp simple vibrations. These are not found in most vibration problems. Hence a simulation and experiment to damp more complex vibrations is useful to implement granular dampers in a wide industrial array.

In the following more possible research of industrial damper optimization are discussed. First, analyzing the dynamic behaviour and draw conclusions to damping efficiency would be a possible and logical next step.

Another possibility to evaluate the dynamic of the granulate is to compare the displacement curves in every detail and draw conclusions from the differing runs as in figure 38.

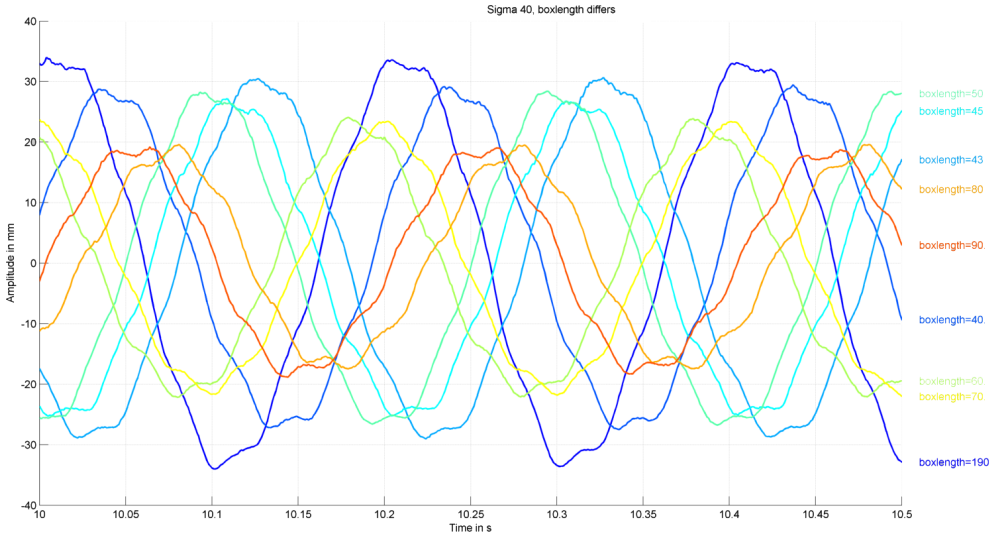


Figure 38: Different dynamic at different vibration patterns of curve for $\sigma_{layer} = 40mm$ and different box lengths

Considering the previous results, an option would be to analyze an industrial application of a damper and create one that uses drive and control technology to allow the optimized damping

of a fluctuating vibration. Nevertheless, during the measurements of the pipe system problems of reproducibility occurred which were ultimately traced back to the pump's setting of the volumetric efficiency and therefore a revision of all hydraulic data was important. Therefore, for simplified future experiments the boundary conditions of the vibration should be as simple as possible.

Different materials such as water or oil (maybe enclosed in small rubber balloons) could also be of interest for further damping research. *Chung* analyzed different standard materials for general damping [11]. The same material investigation could boost the PID technology.

Besides changing the material and with today's 3D printing technology different shapes of granulate could be printed to evaluate the effect of the granulate's shape or structure on damping.

In the numerical field of activity it is possible to create models for a granular damping of different granulates, shapes, box variations, gravity environments (space) and frequencies (even though the models might be very complex). In 2005, *Xu et al.* modeled for example a vibrating plate with inside cavities and confirmed their results with experiments [56]. A continuation of this could be a simulation of a damper on an industrial system before doing experiments at the site. Damages and over-designing due to vibration problems can be found in nearly all technical applications, for example in windmills where extra weight and outages decrease the efficiency and return of investment.

Simulating and designing a damper before a building is in construction would safe money and time in experiments and industrial appliances while receiving improved results.

# 8 Bibliography and list of tables

## References


[1] https://de.wikipedia.org/wiki/Datei:Marinesender_DHO38_L%C3%A4ngstwellensender_der_Marine_-_Zuleitung_%26_Schwingungsd%C3%A4mpfer.jpg#mediaviewer/File:Marinesender_DHO38_L%C3%A4ngstwellensender_der_Marine_-_Zuleitung_%26_Schwingungsd%C3%A4mpfer.jpg, retrieved on 06. Dec. 2014.

[2] http://www.mss.cbi.uni-erlangen.de/KkuDatabase/files/files/1207/Greenscrean-KollmerNeu.mov, retrieved on 06. Dec. 2014.

[3] http://www.cac-chem.de/en/portaldata/1/resources/bilder/galerie/highquality/natural-gas-processing-plant-for-stroytransgaz.jpg, retrieved on 18. Oct. 2014.

[4] http://de.wikipedia.org/wiki/Schwingungsdämpfer, retrieved on 18. Oct. 2014.

[5] Xian-Ming Bai, Leon M Keer, Q Jane Wang, and Randall Q Snurr. Investigation of particle damping mechanism via particle dynamics simulations. *Granular Matter*, 11(6):417–429, 2009.

[6] M. N. Bannerman, J. E. Kollmer, A. Sack, M. Heckel, P. Mueller, and T. Pöschel. Movers and shakers: Granular damping in microgravity. *Phys. Rev. E*, 84:011301, Jul 2011.

[7] Alexander Baumeister. *Lebenszykluskosten alternativer Verfügbarkeitsgarantien im Anlagenbau.* Springer Science+Business Media, 2007.

[8] André Biegner. *Zur Schallemission der selbsttätigen Ventile oszillierender Verdrängerpumpen.* PhD thesis, FAU Erlangen Nuremberg, Lehrstuhl für Apparatetechnik und Chemiemaschinenbau, 1999.

[9] Alfred Böge. *L Kraft- und Arbeitsmaschinen.* Springer Fachmedien Wiesbaden, 2013.

[10] Nikolai V. Brilliantov, Nicole Albers, Frank Spahn, and Thorsten Pöschel. Collision dynamics of granular particles with adhesion. *Phys. Rev. E*, 76:051302, Nov 2007.

[11] DDL Chung. Review: Materials for vibration damping. *Journal of Materials Science*, 36(24):5733–5737, 2001.

[12] B Cipra, P Dini, S Kennedy, and A Kolan. Stability of one-dimensional inelastic collision sequences of four balls. *Physica D: Nonlinear Phenomena*, 125(3):183–200, 1999.

[13] Peter Constantin, Elizabeth Grossman, and Muhittin Mungan. Inelastic collisions of three particles on a line as a two-dimensional billiard. *Physica D: Nonlinear Phenomena*, 83(4):409–420, 1995.

[14] Babak Darabi. *Dissipation of vibration energy using viscoelastic granular materials.* Phd, Department of Mechanical Engineering, University of Sheffield, April 2013.

[15] W. Dettinger. Druckschwankungen und ihre dämpfung in rohrleitungen oszillierender verdrängerpumpen. *Chem.-Technik 13*, (10):61–74, 1984.

[16] Yanchen Du and Shulin Wang. Modeling the fine particle impact damper. *International Journal of Mechanical Sciences*, 52(7):1015–1022, 2010.

[17] Sergei E. Esipov and Thorsten Pöschel. The granular phase diagram. *Journal of Statistical Physics*, 86(5-6):1385–1395, 1997.

[18] Bryce L Fowler, Eric M Flint, and Steven E Olson. Design methodology for particle damping. In *SPIE's 8th Annual International Symposium on Smart Structures and Materials*, pages 186–197. International Society for Optics and Photonics, 2001.

[19] Randolph Danner Friend and VK Kinra. Particle impact damping. *Journal of Sound and Vibration*, 233(1):93–118, 2000.

[20] Jörn Oprzynski ; Eberhard Futterer. *Die Bedeutung der Rohrleitungssysteme in der Prozeß- und Anlagentechnik.* Number 6. Ausgabe in Handbuch Rohrleitungstechnik. Vulkan-Verlag Essen, 1994.

[21] W. Geidel, W.; Arlt. Übersicht zu besonderheiten der rohrleitungsplanung in der chemischen industrie. *3R International 37*, Heft 7:413–417, 1998.

[22] Jürgen Giesecke, Emil Mosonyi, Jürgen Giesecke, and Emil Mosonyi. Druckrohrleitungen. *Wasserkraftanlagen: Planung, Bau und Betrieb*, pages 223–316, 2009.

[23] Ulrich Grau. *Haftkräfte und deren Einfluß auf die Kinematik selbsttätiger Ventile oszillierender Verdrängungspumpen.* PhD thesis, 1996.

[24] Margit Hahn. Druckstöße in rohrleitungen: Störungsszenarien, sicherheitsbetrachtungen und gegenmaßnahmen. *Chemie Ingenieur Technik*, 81(1-2):127–136, 2009.

[25] Gordon R.W. Hollkamp, J.J. Passive damping and isolation. In *Proceedings of SPIE Conference on Smart Structures and Materials*, volume vol. 3327(2), CA, San Diego, 1998.

[26] Dr. Ing. Dietmar Jarmer. *Zur Erregung mechanischer Rohrleitungsschwingungen durch oszillierende Verdrängerpumpen.* PhD thesis, Universität Erlangen-Nürnberg, 2002.

[27] KL Johnson, K Kendall, and AD Roberts. Surface energy and the contact of elastic solids. *Proceedings of the royal society of London. A. mathematical and physical sciences*, 324(1558):301–313, 1971.

[28] A Kudrolli, M Wolpert, and Jerry P Gollub. Cluster formation due to collisions in granular material. *Physical review letters*, 78(7):1383, 1997.

[29] Hongming Li. *Impact of cohesion forces on particle mixing and segregation.* PhD thesis, University of Pittsburgh, 2006.

[30] Zheng Lu, Xilin Lu, Wensheng Lu, and Sami F Masri. Experimental studies of the effects of buffered particle dampers attached to a multi-degree-of-freedom system under dynamic loads. *Journal of Sound and Vibration*, 331(9):2007–2022, 2012.

[31] Zheng Lu, Xilin Lu, and Sami F Masri. Studies of the performance of particle dampers under dynamic loads. *Journal of Sound and Vibration*, 329(26):5415–5433, 2010.

[32] Kurt Magnus, Karl Popp, and Walter Sextro. *Freie Schwingungen.* Springer Fachmedien Wiesbaden, 2013.

[33] Sean McNamara and W. R. Young. Inelastic collapse in two dimensions. *Phys. Rev. E*, 50:R28–R31, Jul 1994.

[34] Sean McNamara and W. R. Young. Dynamics of a freely evolving, two-dimensional granular medium. *Phys. Rev. E*, 53:5089–5100, May 1996.

[35] H. Nakasone, Y.; Hara. Fem simulation of growth of fish-eye cracks in the very high cycle fatigue of a high strength steel suj2. In Y. Sakai, T.; Ochi, editor, *Conference on Very High Cycle Fatigue (VHCF-3)*, volume Proc. of the 3rd Intern., pages 40–47. Society of Materials Science Japan, 2004.

[36] J. S. Olafsen and J. S. Urbach. Clustering, order, and collapse in a driven granular monolayer. *Phys. Rev. Lett.*, 81:4369–4372, Nov 1998.

[37] A Papalou and SF Masri. Response of impact dampers with granular materials under random excitation. *Earthquake Engineering and Structural Dynamics*, 25(3):253–268, 1996.

[38] A Papalou and SF Masri. An experimental investigation of particle dampers under harmonic excitation. *Journal of vibration and control*, 4(4):361–379, 1998.

[39] Positive Displacement Pumps-Reciprocating. Api 674, 1995.

[40] George Ramachandran, Sanjiv; esieutre. Dynamics and performance of a harmonically excited vertical impact damper. *Journal of Vibration and Acoustics*, 2008.

[41] M Ben Romdhane, M Trigui, E Foltête, M Haddar, and N Bouhaddi. Vibration passive damping by an intrusive approach. *Vibrations, Shocks and Noise symposium*, 2012.

[42] Achim Sack, Michael Heckel, Jonathan E. Kollmer, Fabian Zimber, and Thorsten Pöschel. Energy dissipation in driven granular matter in the absence of gravity. *Phys. Rev. Lett.*, 111:018001, Jul 2013.

[43] M Saeki. Impact damping with granular materials in a horizontally vibrating system. *Journal of Sound and Vibration*, 251(1):153 – 161, 2002.

[44] M Saeki. Analytical study of multi-particle damping. *Journal of Sound and Vibration*, 281(3):1133–1144, 2005.

[45] Clara Salueña, Thorsten Pöschel, and Sergei E. Esipov. Dissipative properties of vibrated granular materials. *Phys. Rev. E*, 59:4422–4425, Apr 1999.

[46] Dr.-Ing. Manuela Sander. *Einleitung*. Springer Berlin Heidelberg, 2008.

[47] Helmut Schmidt. *Schalltechnisches Taschenbuch*. VDI-Verlag, 1984.

[48] Günter Scholz. Bauarten und wärmetechnische berechnungen von wärmeübertragungsapparaten, wärmespeichern und druckbehältern. In *Rohrleitungs- und Apparatebau*, pages 1–397. Springer Berlin Heidelberg, 2012.

[49] B. Seidl. *Zur Reduzierung der Druckschwingung in Rohrleitungssystemen oszillierender Verdrängerpumpen*. PhD thesis, Lehrstuhl für Apparatetechnik und Chemiemaschinenbau, Universität Erlangen-Nürnberg, 1992.

[50] AS Tijsseling. Fluid-structure interaction in liquid-filled pipe systems: a review. *Journal of Fluids and Structures*, 10(2):109–146, 1996.

[51] H. Tschöke and H. Hölz. *Verdrängerpumpen*. Springer Berlin Heidelberg, 2011.

[52] G Vetter and H Fritsch. Auslegung von pulsationsdämpfern für oszillierende verdrängerpumpen. *Chemie Ingenieur Technik*, 42(9-10):609–616, 1970.

[53] Klaus H. Weber. *Projektvorbereitung und Grundlagenermittlung*. Springer Berlin Heidelberg, 2014.

[54] Jens Wittenburg. Schwingungslehre. *Heidlberg: Springer*, 1996.

[55] C.X. Wong, M.C. Daniel, and J.A. Rongong. Energy dissipation prediction of particle dampers. *Journal of Sound and Vibration*, 319(1–2):91 – 118, 2009.

[56] Zhiwei Xu, Michael Yu Wang, and Tianning Chen. Particle damping for passive vibration suppression: numerical modelling and experimental investigation. *Journal of Sound and Vibration*, 279(3–5):1097 – 1120, 2005.

[57] Michael Yichung Yang. *Development of master design curves for particle impact dampers*. PhD thesis, The Pennsylvania State University, 2003.

[58] Tong Zhou and Leo P Kadanoff. Inelastic collapse of three particles. *Physical review E*, 54(1):623, 1996.

[59] Franz Ziegler. Dynamik fester und flüssiger körper. impulssatz (schwerpunktsatz) und drallsatz (drehimpulsoder impulsmomentensatz) für materielle volumina und kontrollvolumina. In *Technische Mechanik der festen und flüssigen Körper*, pages 317–373. Springer, 1985.

# List of Tables